AN EXPERIMENTAL INVESTIGATION OF BLOCKING IN A HIGH-SPEED, CLOSED WIND TUNNEL USING THE WALL PRESSURE METHOD

Thesis by

Donald Lowell Francis

In Partial Fulfillment of the Requirements

For the Degree of

Aeronautical Engineer

California Institute of Technology

Pasadena, California

1949

Acknowledgement

The author wishes to express his appreciation for the assistance and guidance given him by Mr. Richard W. Bell under whose supervision this investigation was carried out. He also extends his thanks to Dr. Clark B. Millikan for his assistance on technical problems.

ABSTRACT

The purpose of this investigation was to determine the possibility of using a semi-empirical, wall pressure method to determine wind tunnel blocking corrections in the transonic range. Included are axial distributions of velocity increments at the wall in the presence of the wing models. The main results are presented in the form of comparisons of the blockage corrections determined by the semi-empirical method with the blocking corrections obtained by direct calculation. The models used in this investigation were reflection-plane-mounted wings of various sizes and sweep angles and one two-dimensional wing. Data for wings at moderate angles of attack are included, when available.

The results indicate that the corrections obtained by the semi-empirical method agree with those obtained by direct calculation in the range of Mach numbers where agreement is expected. The semi-empirical corrections become rapidly larger than the calculated corrections as the critical Mach number of the wing is exceeded. The magnitudes of the differences in the transonic range are sufficiently large to warrant the application of the semi-empirical method to transonic wind tunnel tests.

TABLE OF CONTENTS

INDEX OF FIGURES

INDEX OF FIGURES (Cont'd)

TABLE 1

Notation

Flow Parameters

M_o = Mach number of the undisturbed working section air stream

ΔM = Increment in Mach number due to presence of model

M_w = Mach number at the wall measured by wall pressure orifice

q_o = Dynamic pressure of the undisturbed working section air stream

= $\frac{1}{2}\rho_o U_o^2$

U_o = Velocity of the undisturbed working section air stream

u = Perturbation velocity due to all images in the direction of U_o

u' = Perturbation velocity due to all images except primary (model) image in the direction of U_o

w = Perturbation upwash velocity at working section wall opposite wing tip due to wing circulation

p_w = Static pressure at the wall

p_{wi} = Static pressure at the wall, model installed

p_{wo} = Static pressure at the wall, clear working section

ρ_o = Density of the undisturbed working section air stream

γ = Ratio of specific heats

= 1.400 for air

β = $\sqrt{1-M_o^2}$

ε = Ratio of perturbation velocity to free stream velocity at any Mach number M_o

= $\frac{u}{U_o}$

ε_∞ = ε far downstream from the model

ε_w = ε due to viscous wake

ε_s = ε due to solid blockage

TABLE 1 (Cont'd)

Geometrical Parameters

S_p = Area of the semi-span wing panel

b_p = Semi-span of wing panel

c = Wing chord

t = Maximum thickness of the wing

AR = Wing aspect ratio considering image wing panel

A_o = Cross-sectional area of the working section

A_B = Cross-sectional area of the model (blocked area, ft^2)

B = Width of the working section

H = Height of the working section

B' = Width of the reoriented working section to allow consideration of a semi-span wing as a full span wing mounted centrally in the reoriented working section

= $2H$

H' = Height of the reoriented working section

= B

x = Axial coordinate in working section, measured in feet, positive downstream from the yaw axis of the metrical system

α = Angle of attack of the wing

Force Coefficients

C_{D_p} = Profile drag coefficient at any Mach number M_o

$$= \frac{\text{Drag}}{q_o S_p}$$

C_L = Lift coefficient at any Mach number M_o

$$= \frac{\text{Lift}}{q_o S_p}$$

TABLE 1 (Cont'd)

Special Notation

$( )_A$ = Quantity at the root chord of the wing

$( )_B$ = Quantity at the wall in the plane of symmetry of the wing directly above or below point A

$( )_C$ = Quantity at the wall directly opposite point A in the spanwise direction

CA = Axial row of orifices in the center (approximately) of the ceiling

LWFA = Axial row of orifices in the center of the lower west fillet

LEFA = Axial row of orifices in the center of the lower east fillet

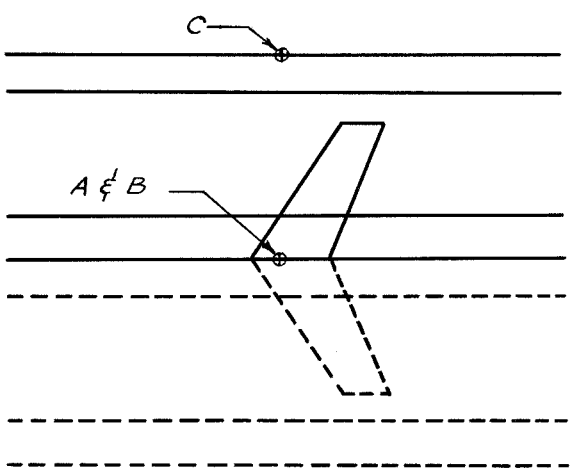

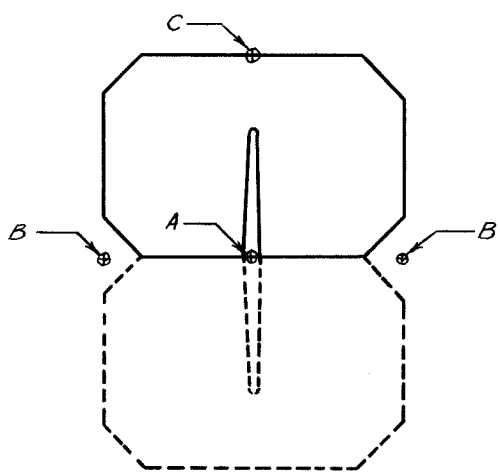

WING CONFIGURATION NOTATION

W_1 = Swept forward, tapered, reflection-plane-mounted wing with small tip fairing

W_2 = Two-dimensional wing spanning working section vertically

W_3 = Straight, tapered, reflection-plane-mounted wing

W_4 = Straight, untapered, reflection-plane-mounted wing

W_5 = Swept back, tapered, reflection-plane-mounted wing

TABLE 2

Model Dimensions

	W_1	W_2**	W_3	W_4	W_5
Semi-span Wing Area, ft^2	9.07	16.95	9.65	5.83	15.99
Semi-span, ft	4.25	8.50	3.62	3.48	6.19
Aspect Ratio*	3.98	∞	2.72	4.16	4.785
Taper Ratio	0.326		0.738	1.000	0.512
Root Chord, ft	3.22	1.99	3.05	1.70	3.44
Tip Chord, ft	1.05		2.25	1.70	1.76
Thickness Ratio of Root Chord	6.0%	12.3%	12.0%	12.0%	9.8%
Thickness Ratio of Tip Chord	5.0%		12.0%	12.0%	9.0%
Sweepback, deg.	-40.0 (45% chord line)	0	0 (25% chord line)	0	37.73 Leading Edge
$\frac{2\,b_p}{B'}$	0.500	1.000	0.426	0.410	0.728
Semi-span Wing Volume, ft^3	1.16	2.74	1.91	0.83	2.94
Maximum Blocked Area, ft^2	0.33	2.08	1.13	0.70	0.84
Location of Max. Blocked Area	x = 3.0	x =0.25	x = 0.4	x = 0	x = 0

---

* Considering reflection-plane image
** Two-dimensional wing spanning the working section vertically

TABLE 2 (Cont'd)

Working Section Dimensions

Height	8.5 ft
Width	12.0 ft
Fillet Chord	$\sqrt{6}$ ft
Cross Sectional Area	96.0 ft^2

AN EXPERIMENTAL INVESTIGATION OF BLOCKING IN A HIGH-SPEED, CLOSED WIND TUNNEL USING THE WALL PRESSURE METHOD

1. Introduction

Wind tunnel blocking may be described as the effect of the finite jet boundaries on the longitudinal components of the flow velocities in the region of the model. For closed wind tunnels at subsonic speeds the longitudinal components are increased by an amount which is essentially uniform over the model, if the model is small enough. This velocity increment is the basis of corrections applied to observed test dynamic pressure, static pressure, and Mach number in order to obtain equivalent values for a model in an infinite stream.

The problem of blocking for incompressible flow has been considered theoretically [1] by dividing the velocity increment into two parts, namely (1) that associated with the physical presence of the model and (2) that associated with the presence of the viscous wake downstream of the model. That part of the velocity increment associated with the solid model is called solid blockage. That part associated with the wake is called wake blockage. When considering solid blockage analytically, the model is replaced with an appropriate distribution of sources and sinks such that the model boundary is sufficiently well represented by this distribution.* The effect of the wall, which is the blockage, is evaluated by replacing the wall with the particular image system of sources and sinks associated with the geometry of the working section and then calculating the increment in velocity at the

---

* It is sufficient only to represent the effect of the model at points no closer to the model than the nearest image

1. Introduction (Cont'd)

model position caused by the images only. The flow outside the wake is approximated by the flow resulting from a source placed at the model position. [2] The wake blockage at first appears to be the increment in velocity at the model position caused by the image sources representing the walls, but this representation does not satisfy the condition that the wake blockage at infinity upstream from the model be zero. The source distribution in the plane of the model would induce a uniform, negative increment at infinity upstream. In order to repair this condition a uniform velocity in the direction of the free stream is superimposed on the source flow so that this negative increment is just cancelled. The wake blockage is then calculated using the combination flow, which yields a uniform velocity increment over the cross section of the working section.

The blockage in a compressible flow can be calculated using the Prandtl-Glauert approximation for small perturbations. There has been confusion in the past regarding the compressible blockage for three-dimensional bodies and wakes, but the situation is clear if the Göthert Extension [3] of the Prandtl-Glauert Rule is used. One of the fundamental problems connected with the compressible blockage corrections is that the velocity range of extreme importance, namely the range: $M_{crit.}$ for the body or wing up to M_{choke} for the tunnel, is also the range in which the corrections calculated directly by the Göthert Extension are no longer applicable. When a region of mixed subsonic and supersonic flow exists around a model, the flow is no longer adequately described by a simple transformation of the body coordinates, hence blocking velocity increments at the model due to the images are not correctly represented. The inadequacy of the description of these blocking velocities has not been caused by linearization of the equations of motion,

1. Introduction (Cont'd)

because the blocking velocity increments are still small compared with U_o. Therefore if the comparison incompressible flow could be altered in some basic way other than by a simple transformation of body coordinates, the blocking corrections could be calculated directly by the Göthert Extension.

Göthert proposed a semi-empirical method for determining the blocking corrections when mixed flow exists around a model. [4] As mentioned above, if the altered incompressible comparison flow were known, then the velocity increments at the model due to the images could be calculated. The velocity increments at the wall due to both the model and the images could be calculated also. These velocities could then be transformed into the compressible flow by the Göthert Extension since these velocities in the compressible flow are small compared with U_o. Both velocities are transformed according to the same relation and hence the ratio of the velocity increment at the wall caused by the model and images to the velocity increment at the model caused by the images alone is the same in both the compressible and the incompressible flow. Therefore, if the velocity increment at the wall in the compressible flow is known, the velocity increment at the model due to the images alone is known also.

The basis of the semi-empirical method is that the blocking velocity at the model may be determined if the blocking velocity at the wall is measured, provided that the ratio of the two velocities is known. The semi-empirical method is essentially the same as the direct calculation method, and therefore it would be expected that the two methods would yield the same results up to $M_{crit.}$ for the model. The results would be expected to diverge for flow Mach numbers greater than $M_{crit.}$. Obviously, even the semi-empirical method is

1. Introduction (Cont'd)

not valid when the blocking velocities at the wall become large compared with U_o, but this occurs at a much higher flow velocity than that at which the occurrence of mixed flow makes the direct calculation difficult.

A great quantity of wind tunnel testing in the transonic range is carried out by many laboratories. This is especially true at the Southern California Cooperative Wind Tunnel [5] (CWT). The semi-empirical method, therefore, has possibilities of wide application at the CWT. It was felt that an experimental investigation of the blocking problem should be carried out before the semi-empirical method could be used with any degree of assurance that the results were more reliable than those of the direct calculation method now used. It seemed desirable to investigate the details of the flow in the working section during routine commercial tests in order to determine the practical aspects of applying the semi-empirical method.

With this investigation in mind, a large number of static pressure orifices were installed in the walls and fillets of the various working sections, so-called "carts," of the CWT. For approximately the last two years of testing (about 100 commercial tests) wall-pressure data have been obtained from these orifices with a variety of model configurations installed in the working section. The various types of configurations included reflection-plane mounts, single-swept-strut mounts, multiple-swept-strut mounts, and sting mounts.

Since very little work in this field has been done, it was felt that configurations with geometrical simplicity should be studied first. The complications that arise from a configuration that includes a swept model-support-strut intersecting a wing-body combination are manifold. The

1. Introduction (Cont'd)

simplest geometry is that of a reflection-plane-mounted wing. This configuration may be treated as a centrally mounted wing with no support struts in a reoriented working section of shape similar to the actual working section. This is possible only in a working section whose width to height ratio is $\sqrt{2}$. With these considerations in mind the great mass of data was sorted and examined for those sets of data which offered the most promise of consistent and accurate results, and at the same time, which covered the range of sizes and shapes of wings likely to be encountered in the future. The reflection-plane-mounted wings chosen for this investigation are a swept forward wing, two straight wings, a swept back wing, and a two-dimensional wing spanning the working section vertically.

Blocking velocity ratios have been determined at the CWT for two-dimensional wings, three-dimensional wings of various sweep angles and span to width ratios, and bodies of revolution all mounted centrally in a working section whose width to height ratio is $\sqrt{2}$.[6] These ratios, therefore, are applicable to the reoriented working section. Two points on the wall are considered, namely B and C as defined in the table of notation.

The analytical calculations were carried out using a line doublet to represent the wings. It should be pointed out that the distribution of sources and sinks used to represent the effect of the wing is adequate if it accurately represents the effect at the wall. This is a more stringent restriction upon the distribution than was imposed on the distribution used to calculate the blocking velocity at the model due to the images. (see footnote, page 9)

1. Introduction (Cont'd)

A few characteristics of the blocking velocity ratios should be noted here. The points B and C, for swept wings, are actually defined as points on the wall in the plane which contains the apex of each swept image doublet. B and C for straight wings lie in the plane of the line sources. For a given wing, the choice of the axial location of the points B and C is a matter of judgement since an estimate must be made of the location of the line doublet or source that best represents the wing. The ratios apply only at points B and C, and not upstream or downstream from those points. With this restriction, the ratios at a given Mach number for a swept back wing, a swept forward wing, and a yawed wing are the same provided that the span to width ratios and the sweep and yaw angles are the same. For a given straight wing or body of revolution, the blocking velocity ratios are independent of Mach number since the lateral dimension to width ratio remains constant in the transformation, and there is no sweep effect. For a given swept wing in compressible flow, however, the blocking velocity ratios are a function of Mach number, since the sweep angle is changed in the transformation, although the span to width ratio remains constant.

It would be helpful in formulating the aims of this investigation if the expected flow characteristics in the working section were described on the basis of the foregoing theoretical background. Considering a series of points on the wall extending from far upstream to far downstream from a straight wing mounted in the working section, the expected velocity increments due to the solid model and its images would at first become negative and decrease until a minimum was reached at some point ahead of the wing, and then rapidly increase up to a peak value in the region opposite

1. Introduction (Cont'd)

the point of maximum blocked area of the model. The increments downstream from this point would decrease, become negative, and reach a minimum at some point downstream of the model. From this point on downstream the increments should approach zero asymptotically. Superimposed upon this distribution is the wake blockage distribution. The wake blockage should be zero far upstream, gradually increase to the value of ε_{w_A} at the model, continue increasing downstream, and asymptotically approach a value of $2\varepsilon_{w_A}$. The combination of these two distributions should not differ much from the solid blockage distribution forward of the model; nor should the addition of the wake blockage change the position of the peak appreciably. The distribution downstream of the model might be changed, however, such that the total velocity increment at the wall would always be positive. For all practical purposes, at some point downstream from the model the blockage should be constant at a value of $2\varepsilon_{w_A}$.

The nature of the distribution for a swept wing would be difficult to predict due to the geometrical complications. The flow pattern probably would ressemble a straight wing pattern with some distortion, but the relative magnitudes of ε and the positions of the peaks and minimums at the fillets and the ceiling would depend on geometry to such an extent that few generalizations could be made.

The axial variation of the velocities at the wall is important if the semi-empirical method is to be applied. If large gradients occur in the region of points B and C, large errors could result from a small error in the choice of the points at which the blocking velocities are measured.

1. Introduction (Cont'd)

With the foregoing considerations in mind, the following phases of the blocking problem were studied:

1. Determine the axial variation of the blockage at the wall in order (a) to establish the possibility of measuring wake blockage at an orifice downstream from the model, and (b) to obtain an estimate of the possible error due to an incorrect choice of the orifices to measure the total blockage at the wall
2. If the possibility of measuring wake blockage is established, compare the measured values with the values computed from the drag measurements on the model
3. Compare the values of blockage at the model computed from wall measurements (semi-empirical method) with the values computed from model dimensions and low speed drag data (direct calculation method)
4. Determine the variation of total blockage at the model with Mach number and angle of attack
5. If differences exist between measured and computed blockage corrections, determine the significance of these differences as regards the final model characteristics.
6. Investigate the effects of sweepback and span on the blocking characteristics.

This investigation can not determine whether the methods applied arrive at the correct blockage.

2. Description of the Experimental Apparatus

The three-dimensional wings were mounted so that the model plane of symmetry coincided with the working section floor. The two-dimensional wing was mounted in the conventional manner. All models were mounted so that the drag on the portion of the model in the boundary layer was measured by the metrical system, but that no forces on the fairing plates were measured.

The static pressure orifices are located in axial rows along the various walls and fillets of the working section. (cf. Fig. 2) The spacing between the orifices in a given row is approximately 1 foot. Pains were taken to have the wall in the immediate region of each orifice free from surface irregularities. A great deal of attention cannot be given to the maintenance of the surface smoothness of the walls; hence the data obtained from these pressure orifices have to be classed as strictly operational.

The walls and fillets of the working section have surface waves in them and consequently the axial variation of static pressure appears very jagged in many cases. This is a source of complication in the data reduction procedure. The technique of compensating for the waves is described in the Description of the Data Reduction.

The flow conditions in the working section are determined by pressures measured by two piezometer rings upstream of the working section. The ring in the maximum diameter section of the tunnel just upstream of the convergent section measures a pressure called P_1. The ring located just upstream of the end of the convergent section measures a pressure called P_2.

The wall-pressure measurements are recorded by photographing a 108-tube-multiple-manometer with a 35 mm. camera. This multiple-manometer has

appearing on it the reference pressures, P_1 and P_2. This fact permitted the reduction of the pressures measured on this manometer into readily usable form without the knowledge of the manometer fluid density. The photographic distortion is minimized by careful alignment of the manometer with the camera and by the use of a high quality camera. The porthole through which the photographs are taken is of optical quality. Complete wall-pressure measurements were obtained only for the three-dimensional wings.

The wall-pressure measurements obtained for the two-dimensional wings were restricted to one pressure opposite the wing on the east wall. This pressure was measured by a micromanometer. The pressure at this same orifice was measured with a micromanometer for the clear working section configuration. The wall-pressure measurements for the two dimensional wing are probably accurate within 0.02 cm of Acetylene Tetrabromide (specific gravity = 2.95). Obviously these measurements are much more refined than those obtained by photographically recording fluid heights on a multiple-manometer. Complete wall-pressure measurements for the two dimensional wing were not available.

The piezometer ring pressure difference, P_1-P_2, is measured and recorded automatically by a Tate-Emery Indicator and a IBM follow-up unit. The downstream ring pressure, P_2, is measured on a vacuum-reference Mercury micromanometer. The absolute pressure of the vacuum is measured on a standard Pirani gauge. The accuracy of the Tate-Emery Indicator is within 0.2 lb/ft^2, and the accuracy of the micromanometer is within 0.01 cm of Mercury. The combined accuracy of the measuring instruments is adequate to determine the Mach number in the working section within 0.002 and the dynamic pressure within 0.25 percent.

3. Description of the Data Reduction

The wall pressures were reduced to values of Mach number. The manometer photographs in negative form were projected onto the ground glass of a Recordak. A device, which included a horizontal hair-line, was attached to the Recordak over the ground glass. The hair-line could be moved up and down while remaining parallel to an initial position. The position of this hair-line was indicated by the position of a center tap on a slide-wire. This slide-wire formed two legs of a Wheatstone Bridge, and the bridge unbalance was measured on a Brown potentiometer. In short, the Brown potentiometer indicated the position of the hair-line. Through the use of the reference tubes on the manometer and a non-linear scale on the potentiometer, the wall Mach numbers could be read directly from the potentiometer scale simply by placing the hair-line even with the top of the fluid column image on the ground glass.

Each manometer photograph was identified with a definite working section Mach number, M_o, measured by the piezometer rings. This permitted the preparation of plots of M_w vs. M_o for each orifice in the working section. This was done for both "clear" and "model installed" working section configurations. The increment in M_w due to the model was determined from these plots at constant values of M_o. This procedure eliminated the effects of the surface waves in the working section walls to a first approximation at least. The clear working section plots were essentially calibrations of each orifice.

The increment, ΔM_w, was tabulated vs. x, the axial coordinate of the orifice. Values of ε were computed using the following relation.

$$\varepsilon = \frac{\Delta M_w}{M_o} \quad \frac{1}{1 + 0.2\, M_o^2}$$

These values of ε at the wall were then plotted vs. x with either angle

3. Description of the Data Reduction (Cont'd)

of attack or M_o as a parameter (see Figs. 8-11)

The wall pressure data for the two-dimensional wing were reduced in a much simpler fashion. The micro-manometer readings were converted into the following dimensionless ratios,

$$\frac{P_2 - P_{w_i}}{P_1 - P_2} \quad \text{and} \quad \frac{P_2 - P_{w_o}}{P_1 - P_2}$$

These ratios were then plotted vs. M_o and differences obtained at constant values of M_o. These differences were then converted to $\frac{P_{w_o} - P_{w_i}}{q_o}$ using values of $\frac{P_1 - P_2}{q_o}$ obtained from the flow calibration of the wind tunnel. The value of ε at the wall is then $\frac{P_{w_o} - P_{w_i}}{2q_o}$ if the small perturbation theory is valid.

4. Evaluation of the Experimental Results

A. The Axial Variation of Blockage at the Wall.

The data presented for W_1 (Figs. 8a and 8b) seem fairly reasonable with a few exceptions. The variation of ε with x is irregular since the values should approach zero asymptotically instead of becoming positive again as x approaches - ∞. A possible explanation is that the boundary layer growth in the working section may have changed during the period of time (3 months) between the "model in" tests and the "clear working section" tests. This could cause a general shift in the measured values of ε in any region of the working section. It should be noted that a ΔM_w of 0.001 corresponds approximately to 1 mm on the plot. The LWFA orifice at x = 6 evidently was radically changed in the three month period. These data do indicate, however, that the flow above and below the wing was fairly symmetrical. It is obvious that measurements were not obtained far enough from the model to separate the solid blockage from the wake blockage. The predominant factor in estimating the position of maximum ε at the wall is the position of maximum blocked area (see Fig. 3), although the peak on the ceiling is slightly forward of the peak on the fillets except when M_o approaches $M_{o_{choke}}$. The large gradients indicate the possibility of error in the measurement of the blockage at the wall.

The measured values of ε for W_3 seem very reasonable (see Fig. 9). The value of α for zero lift indicated by the wall pressures is -1.1°, while the value obtained from the lift curve is -1.2°. The region of solid blockage seems to be defined for $\alpha = 0°$, but not for $\alpha \neq 0°$. The peak value of ε is directly opposite the maximum blocked area position, as would be expected. There is no explanation for the ragged appearance of the CA data.

4. Evaluation of the Experimental Results (Cont'd)

The data for W_4 (Fig. 10) appear to have small scatter, but they appear irregular in other respects. The relative magnitudes of ε for the ceiling and the fillets do not agree too well with those for W_3, even though the two wings are very similar. The gradients appear to be small enough that the blocking obtained from measurements at the wall should be reliable at all but the highest Mach number. These data were used to compare measured wake blockage with computed wake blockage because the solid blockage seems to be negligible at $x = 6$ for all but the highest Mach numbers.

The data for W_5 (Figs. 11a, 11b, and 11c) show very clearly that the position of the maximum blocked area is not the predominant factor in determining the position of the peak ε at the wall for a swept wing of this size. The peak at the ceiling is 2 ft downstream from the peak at the fillets. The gradients shown in these data indicate that large errors may exist in the measured blockage.

B. The Comparison of Measured and Computed* Wake Blockage

Fig. 12 shows the comparison obtained for W_4. Something is radically in error because even the orders of magnitude do not agree at $M_0 = 0.70$. The agreement is better at the higher Mach numbers, but it seems apparent that the whole level of ε is in error downstream of the model.

Fig. 13 shows the comparison obtained for W_5 at various angles of attack. These data show only a factor of 2 difference at $\alpha = 0^\circ$ and a much larger difference at $\alpha \neq 0^\circ$. Note that the CA orifice measured the greatest difference from the computed value. This orifice probably measured a solid blockage increment due to the wing tip. This fact indicates that only those data for $\alpha = 0^\circ$ are possibly valid as a comparison. The

---

* Equations for computing wake blockage are summarized in the Appendix.

4. Evaluation of the Experimental Results (Cont'd)

$\alpha = 0^\circ$ data indicate that (1) the equation

$$\varepsilon_{w_A} = \frac{C_{D_p} \quad S_p}{4\beta^2 \, A_o}$$

is not satisfactory to compute ε_w, (2) that the value of ε_w at x = 6 is not equal to the wake blockage at a greater distance downstream, i.e., twice the blockage at the model, or (3) the orifice at x = 6 measured some solid blockage. It is highly improbable that inaccuracies of measurement are responsible for the lack of agreement, since measured values are always higher than computed values. It seems most reasonable, assuming that the equation is correct, that the lack of agreement is due to the orifices measuring some solid blockage. The situation cannot be resolved by any further analysis of these data.

C. The Effect of Mach Number on the Comparison of Measured and Computed* Total Blockage at the Model

Before discussing the results of this phase of the investigation it would be advantageous to describe the procedure used in obtaining blockage at the model from measured values of ε at the wall. The procedure used was outlined in Reference 4, but the completion of Reference 6 has permitted a slightly more refined technique to be used in this work.

In the procedure that follows, wake blocking is always determined using the equation

$$\varepsilon_w = \frac{C_{D_p} \quad S_p}{4\beta^2 \, A_o}$$

The solid blocking at the wall is determined by subtracting out the wake blocking.

$$(\varepsilon_s)_{B \text{ or } C} = \varepsilon_{B \text{ or } C} - \varepsilon_w$$

---

* See the Appendix

4. Evaluation of the Experimental Results (Cont'd)

The solid blockage at the model is then computed using the relation

$$(\varepsilon_s)_A = (\varepsilon_s)_{B \text{ or } C} \cdot \frac{u_A'}{u_{B \text{ or } C}} .$$

The addition of the wake blockage yields the total blockage at the model.

$$\varepsilon_A = (\varepsilon_s)_A + \varepsilon_w$$

The values of ε_B for W_3 and W_5 at various angles of attack were obtained by averaging the values above and below the wing. This procedure is probably satisfactory as long as the small perturbation theory holds. The calculations to determine ε_C for W_5 involved a more elaborate procedure to account for the velocity increments induced by the wing circulation. The values of w, the upwash velocity at point C, were calculated by replacing the lifting, semi-span wing with two point doublets.[7] The locations and strengths of the doublets were determined so that the lift and rolling moment about the root chord line for the doublets matched the measured lift and rolling moment of the wing. The induced velocity at point C was then computed considering both the image doublets and the primary (model) doublets, whereas the image doublets only were considered in reference 7. The use of two doublets instead of a more refined system was a crude approximation, but the effect of any errors in this approximation on the final result was small since $(\frac{w}{U_o})^2$ was less than $(0.004)C_L^2$ for the incompressible case. The compressible correction term was always less than 3 percent of the measured value of ε at the wall. The correction could probably be neglected for wings the size of W_3 or W_4.

The semi-empirical method cannot separate the effects of wake blockage from the solid blockage. Since both total and solid blockage include

4. Evaluation of the Experimental Results (Cont'd)

the effects of wake blockage, the results of the semi-empirical method were presented in the form of total blockage in order to make a direct comparison with the direct calculation method now used at the CWT.

The comparison of measured and calculated values of total blockage for W_2, the two-dimensional wing, shows fair agreement up to the $M_{crit.}$ for the wing (approximately $M_o = 0.74$), if the points at $M_o = 0.30$ and $M_o = 0.40$ are not weighted too heavily (Fig. 15a). These points are less reliable than those at the higher Mach numbers due to inherent experimental difficulties. If these two points are ignored, the measured values vary with Mach number very nearly as $\frac{1}{\beta^3}$ which is predicted by the direct calculation method. The measured values become increasingly larger than the calculated values as Mach number increases above $M_{crit.}$. This effect was predicted by Thom in reference 1.

Fig. 14 shows the comparison of measured and calculated values of blockage for W_1, the swept forward wing. Appearing in this figure are two curves obtained by the direct calculation method. The upper curve was calculated on the basis of volume only. The calculation of the lower curve used the same wing volume, but it also included a correction due to sweep. This correction was evaluated in reference 6. The magnitudes of the values and the variation with Mach number of the latter curve agrees very well with the semi-empirical curve. The $M_{crit.}$ for the wing is approximately $M_o = 0.90$. A possible cause of the difference between the two semi-empirical curves is the effect of the working section fillet. The curve from position B was obtained from measurements at points on the fillets approximately 0.85 ft from the wall, and no correction was applied to compensate for this.

4. Evaluation of the Experimental Results (Cont'd)

Results of reference 1 predict that the position B curve should fall above the position C curve.

The comparison of the measured and computed values of blockage at the model for W_4, a straight three-dimensional wing, is shown in Fig. 17. The magnitudes of the values obtained by the two methods agree fairly well, but the variation with Mach number obtained by the semi-empirical method does not agree with that of the direct calculation method. The latter result should be viewed with care, however, because the measured values were not obtained over a large enough range of Mach numbers to adequately establish the variation with Mach number. $M_{crit.}$ for the wing is approximately $M_o = 0.78$. These results show the rapid divergence between the two methods above $M_{crit.}$.

Fig. 18 shows the comparison for W_5, the swept back wing, at several angles of attack. The agreement between the values obtained by the two methods is poor, but this would be expected for a wing of this size. It does not seem reasonable that the representation of the effect of the wing at the wall by a line doublet would adequately describe the blocking velocities, even below the $M_{crit.}$ (approximately $M_o = 0.85$) for the wing.

The comparison of the results of the two methods for W_3, a straight three-dimensional wing, is shown on Fig. 16. There is little agreement between the two methods, but this fact may be partially explained by the effect of the fillet, as mentioned in the discussion for W_1. These data are not extensive enough to allow any conclusions to be drawn.

4. Evaluation of the Experimental Results (Cont'd)

D. The Effect of Angle of Attack on the Comparison of Measured and Computed Total Blockage at the Model

Figs. 16, 17, and 19 present the results of this phase of the investigation. The measured values of blockage increase with angle of attack, which is to be expected. Fig. 19 shows that the variation is approximately the same for different Mach numbers, but these data are so sketchy and erratic that no satisfactory conclusions can be made.

E. Significance of Observed Differences between Measured and Computed Blockage

The wake blockage discussion to follow is concerned with data obtained for W_5 only since the data for W_4 are very likely to be erroneous. Fig 20a shows the increments in Mach number, ΔM_A*, and dynamic pressure, Δq_A*, which would result from differences between the computed wake blockage and the wake blockage measured at LEFA, x = 6 (See Fig. 13) for W_5, $\alpha = 0°$. It is assumed here that the solid blockage could be determined without using any value of wake blockage. If the two different values of wake blockage were used to determine the solid blockage, the increments in Mach number and dynamic pressure would be just the factor $(1 - \frac{u_A'}{u_B})$ times those shown in Fig. 20a. Clearly the increments are negligible until the onset of choking, when the increments increase rapidly to maximum values of $\frac{\Delta q_A}{q_o} = 0.6\%$ and $\Delta M_A = 0.005$. Since the uncertainties of wind tunnel data

- - - - - - - - - - - - -

* The equations used to compute these values are given in the appendix

4. Evaluation of the Experimental Results (Cont'd)

are large for conditions near choking, it seems that the observed differences are not significant for most cases. The wake blockage computed from measured drag on the model should be satisfactory, especially since the procedure is much simpler.

The observed differences between measured and computed total blockage cause larger increments in Mach number and dynamic pressure (See Fig. 20b). The differences used to compute the increments on Fig. 20b are those observed for W_2, $\alpha = 0^\circ$ (Fig. 15). These data were used because they are the most accurately measured blocking data in this investigation, and they show large differences. The data for other wings at $\alpha = 0^\circ$ show smaller differences and are less reliable. Differences observed for wings at $\alpha \neq 0^\circ$ were not considered. The increments are definitely negligible up to $M_{crit.}$ (approximately $M_o = 0.74$) and increase rapidly as this Mach number is exceeded. The consequences of these increments are significant since (1) the corrected test Mach number, using computed values of blockage, corresponding to the steep drag rise would be low by approximately 0.01, and (2) the coefficients measured would be approximately 1.5% too large. The effects of these increments are accumulative, not compensating.

5. Conclusions

The results obtained for the two-dimensional wing indicate that the blocking corrections determined by the semi-empirical method closely approximate the magnitudes and the variation according to the $\frac{1}{\beta^3}$ law of the corrections obtained by direct calculation up to the critical Mach number of the wing. As predicted in reference 1, the semi-empirical corrections become rapidly larger than the calculated correction as the $M_{crit.}$ for the wing is exceeded.

The results obtained for the swept forward wing indicate that the semi-empirical blocking corrections agree very closely with the corrections obtained by direct calculations including the effect due to sweep. This result verifies quantitatively the dependence of blockage on Mach number, as predicted in reference 6, for a swept wing.

The results obtained for the large swept back wing do not show the same agreement as do the results for the swept forward wing. This model may be too large to be represented adequately by a line doublet. The results for the other wings were so limited in their scope that no conclusions as to agreement between the semi-empirical and the directly calculated corrections could be formed.

The results of the wake blockage investigation do not indicate any agreement between calculated values and values measured at less than one tunnel height downstream from the model. The differences observed are sufficiently small that their effects on the corrected test Mach numbers and dynamic pressures are negligible.

5. Conclusion (Cont'd)

The observed differences between semi-empirical and calculated values of total blockage in the transonic range are sufficiently large to affect significantly the final model coefficients.

The results shown here represent information regarding the problem of blocking corrections for the simplest model configurations in the transonic range . Future investigations should include the more complicated configurations, especially those involving a model support strut.

References:

1. Thom, A., "Blocking Corrections in a Closed High-speed Tunnel", R. & M. 2033

2. Durand, W. F. (Editor-in-Chief), Aerodynamic Theory, Vol. III, page 195

3. Göthert, B., "Plane and Three-dimensional Flow at High Subsonic Speeds", NACA TM 1105

4. Göthert, B., "Windkanalkorrekturen bei hohen Unterschallgeschwindigkeiten unter besonderer Berücksichtigung des geschlossenen Kreiskanals", Deutsche Versuchsanstalt für Luftfahrt, Forschungsbericht Nr. 1216

5. Millikan, C. B., Smith, J. E., and Bell, R. W., "High-Speed Testing in the Southern California Cooperative Wind Tunnel", Journal of the Aeronautical Sciences, Vol. 15, No. 2 (February, 1948)

6. Hensel, R. W., "Rectangular Wind Tunnel Blocking Corrections Using the Velocity Ratio Method", CWT Rep. T-20

7. Katzoff, S. and Hannah, M. E., "Calculation of Tunnel-Induced Upwash Velocities for Swept and Yawed Wings", NACA TN 1748

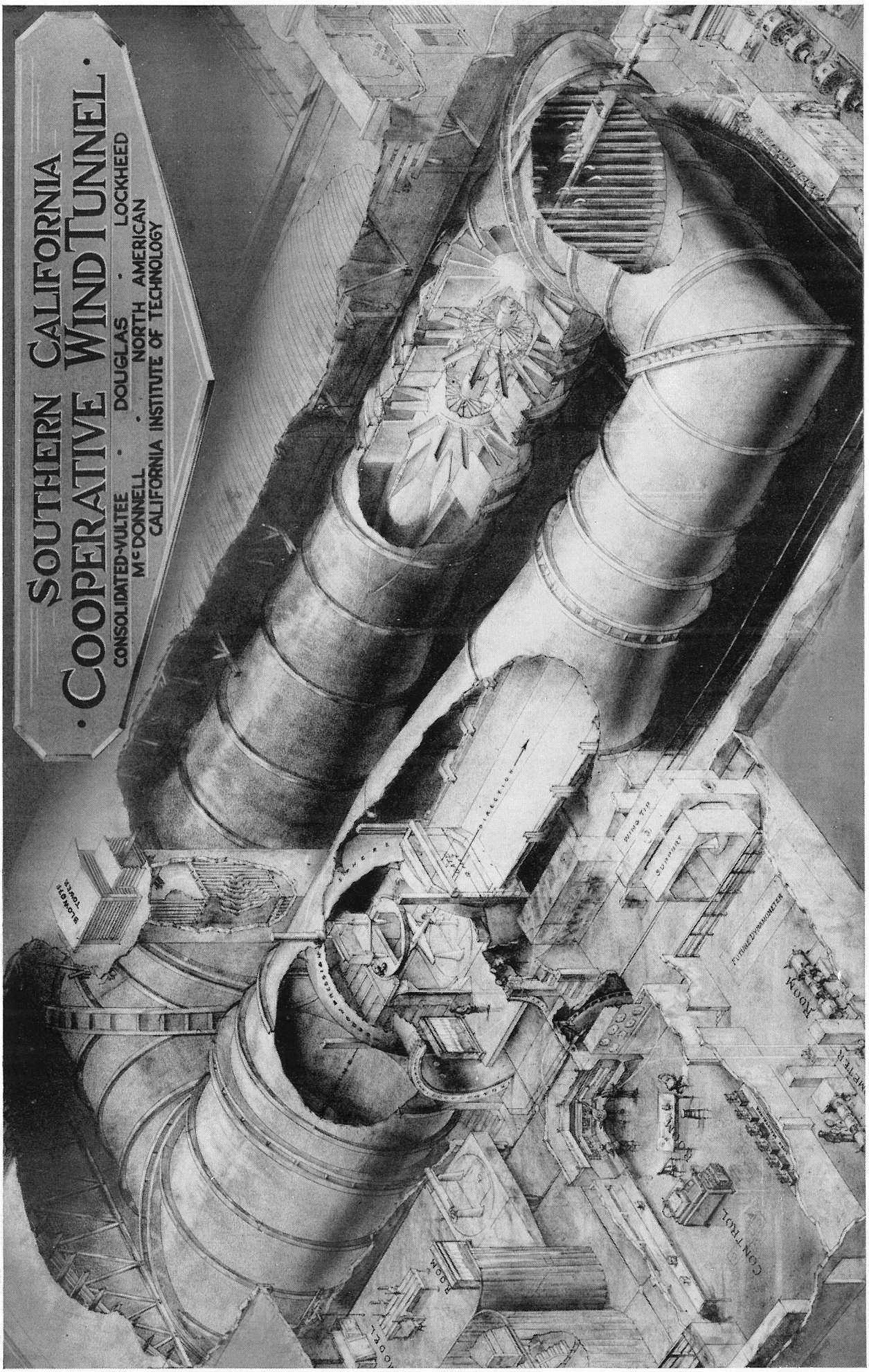

Fig. 1 Cutaway Drawing of the CWT

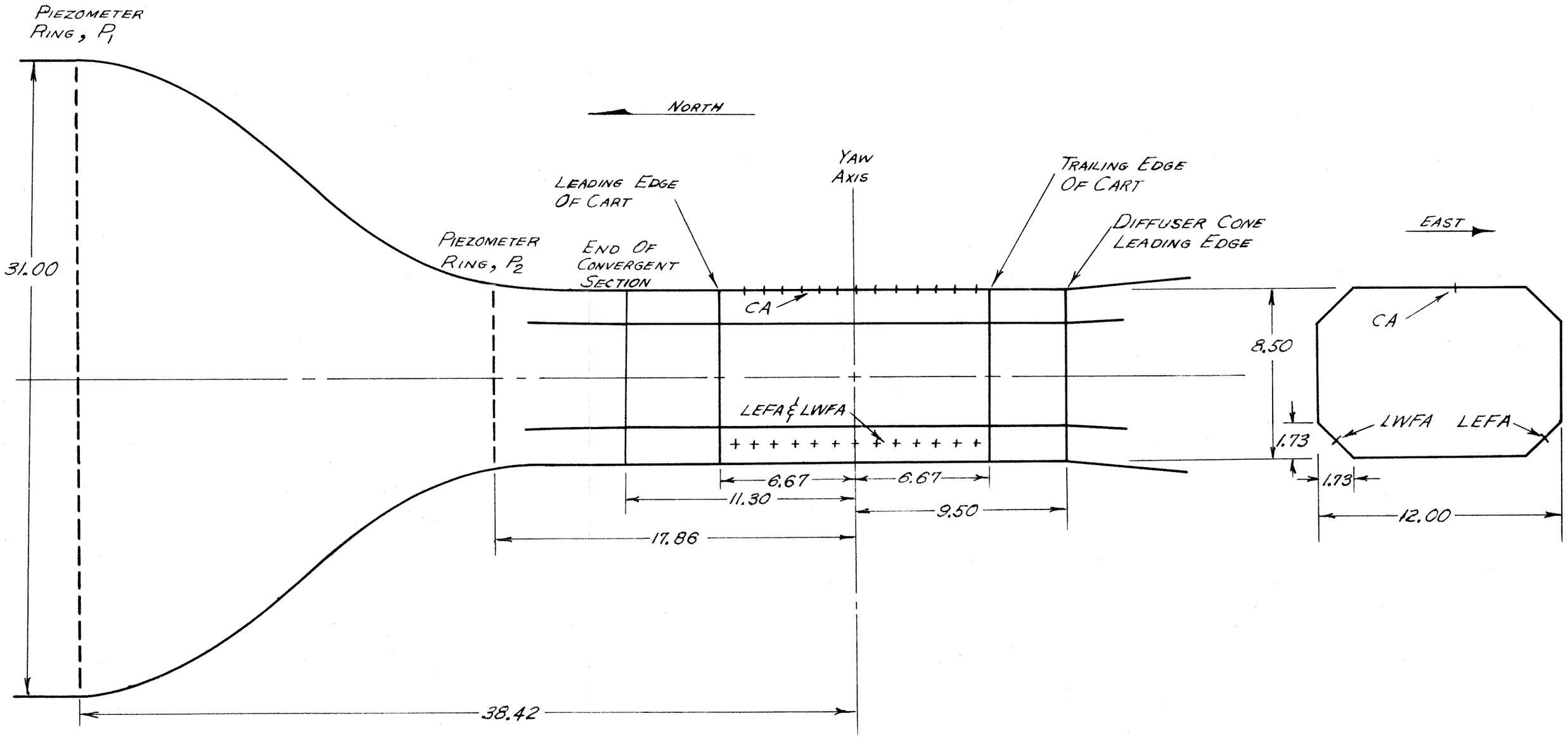

FIG. 2 SKETCH SHOWING THE WORKING SECTION REGION OF THE CWT

NOT TO SCALE
ALL DIMENSIONS IN FEET

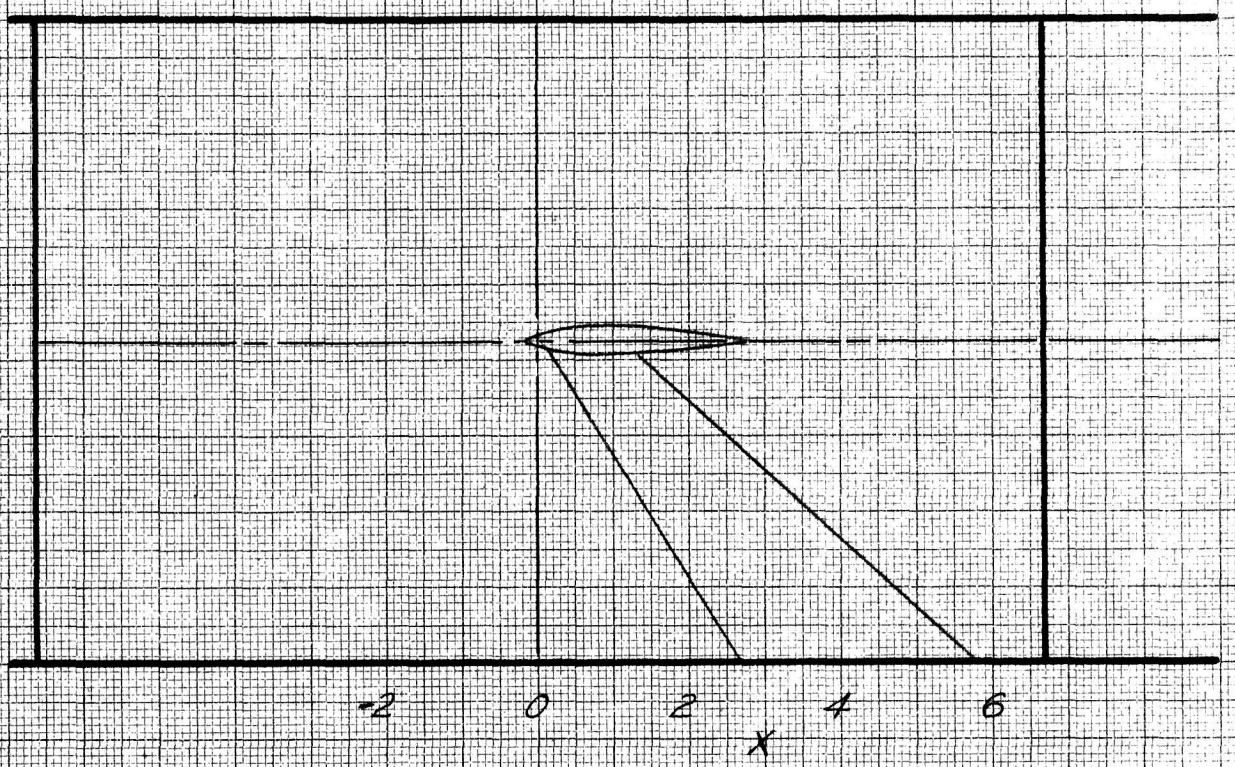

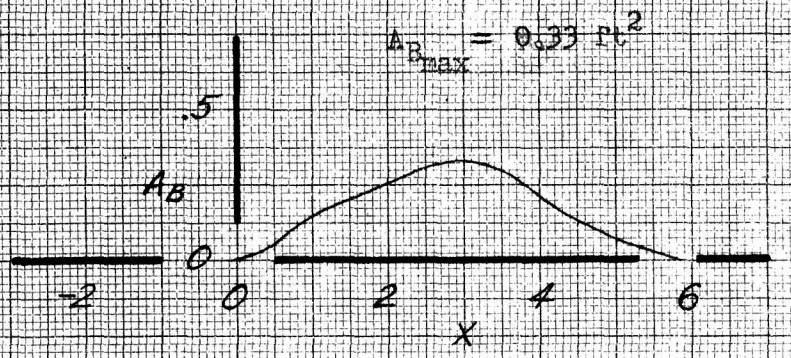

Fig. 3 Sketch of Model Installation and Plot of the Blocked Area Distribution for W_1

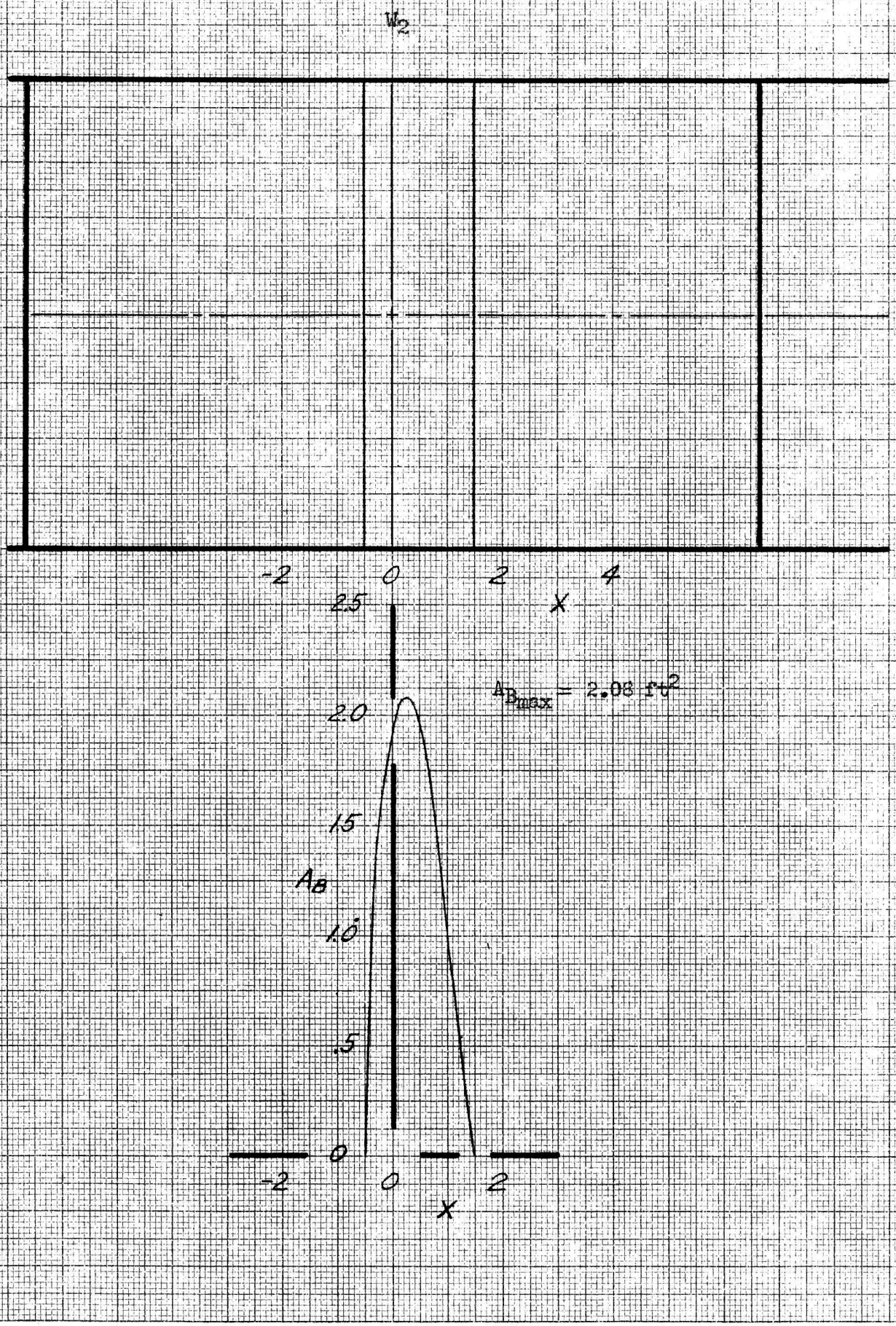

Fig. 4 Sketch of the Model Installation and Plot of the Blocked Area Distribution for W_2

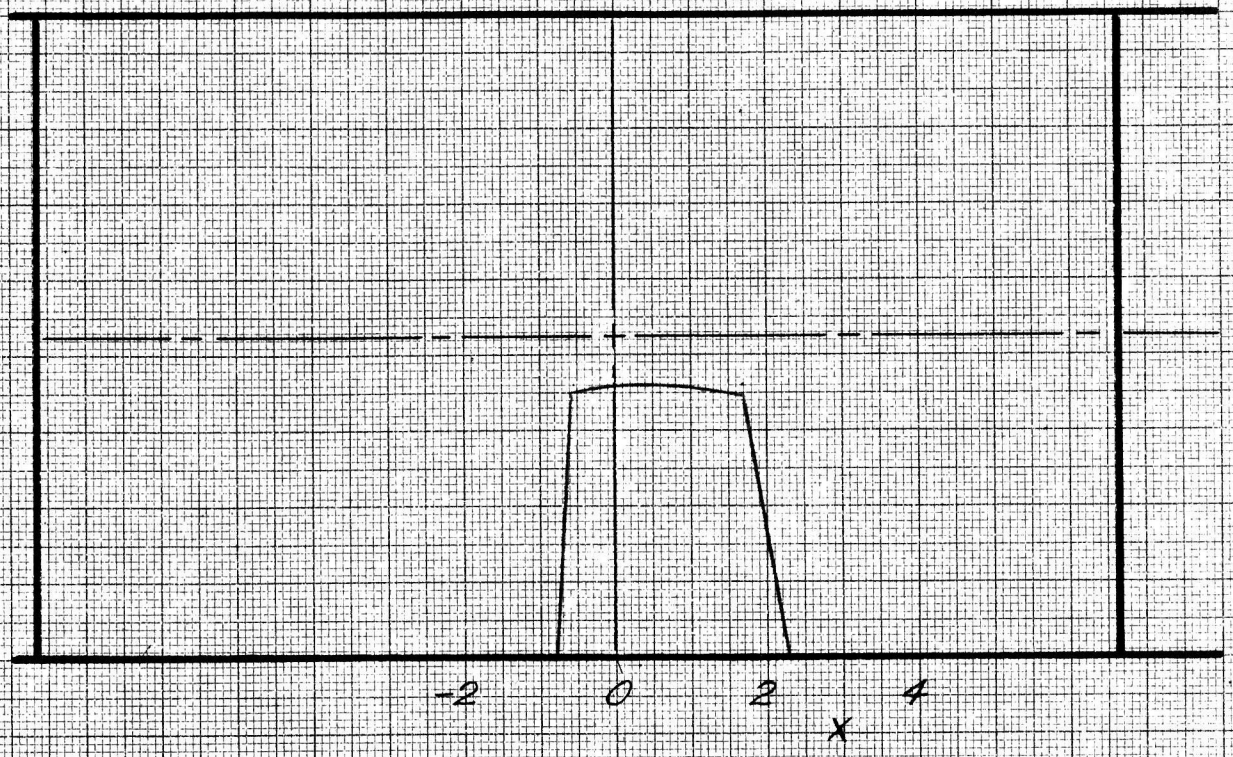

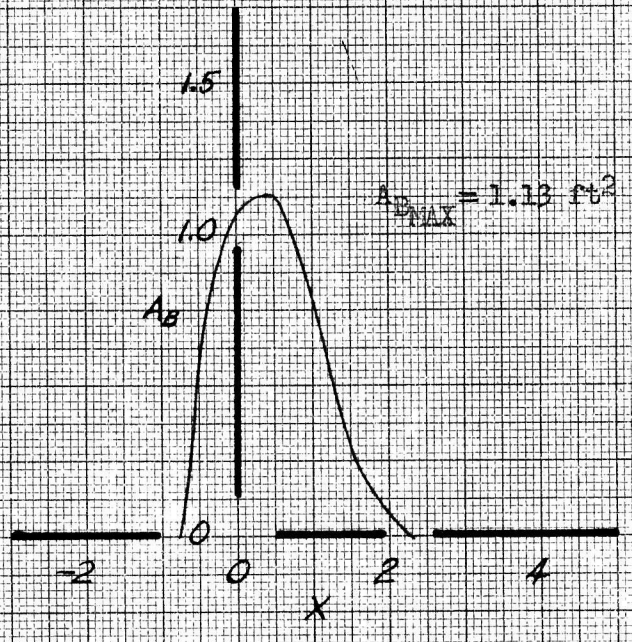

Fig. 5 Sketch of the Model Installation and Plot of the Blocked Area Distribution for W_3

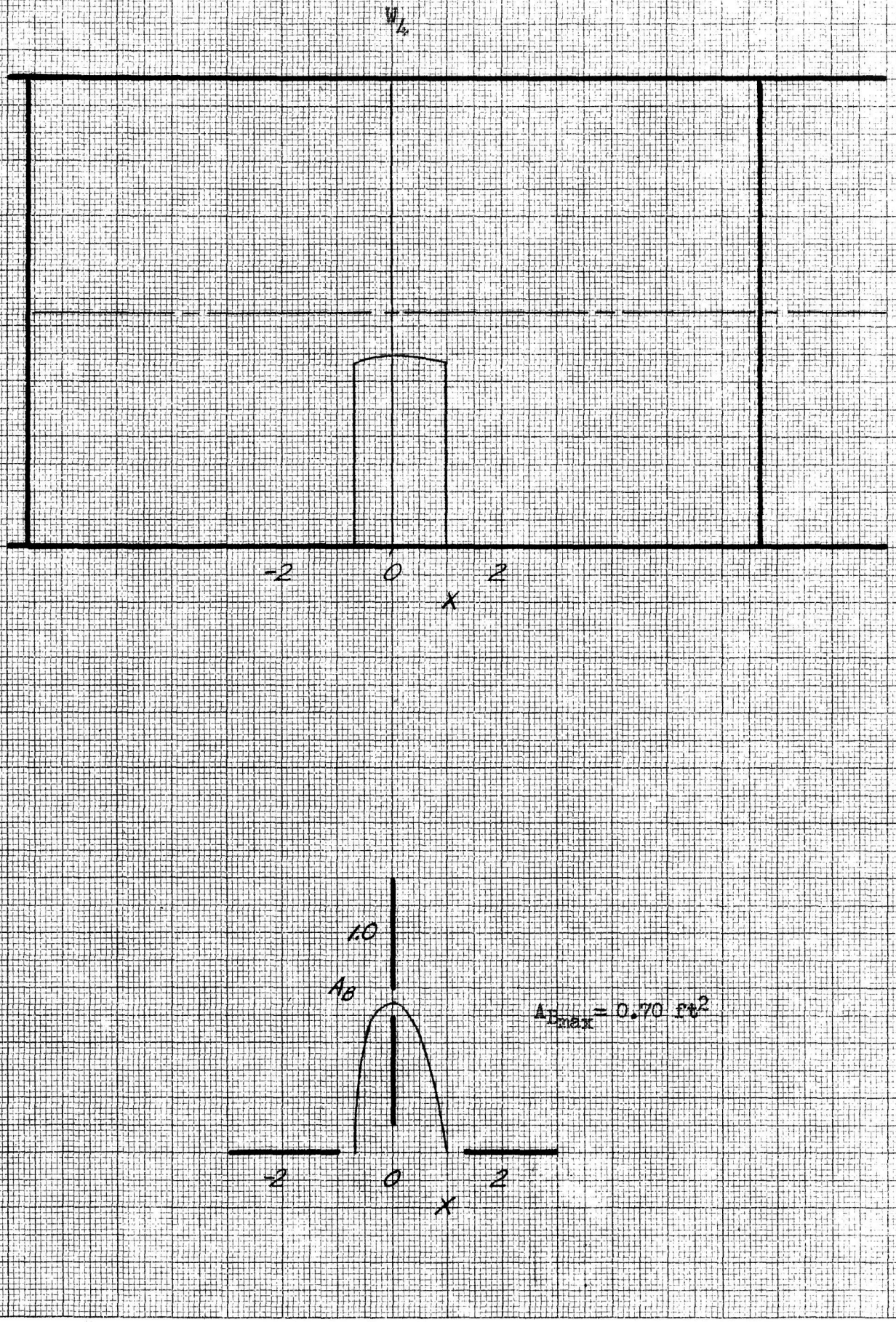

Fig. 6 Sketch of the Model Installation and Plot of the Blocked Area Distribution for W_4

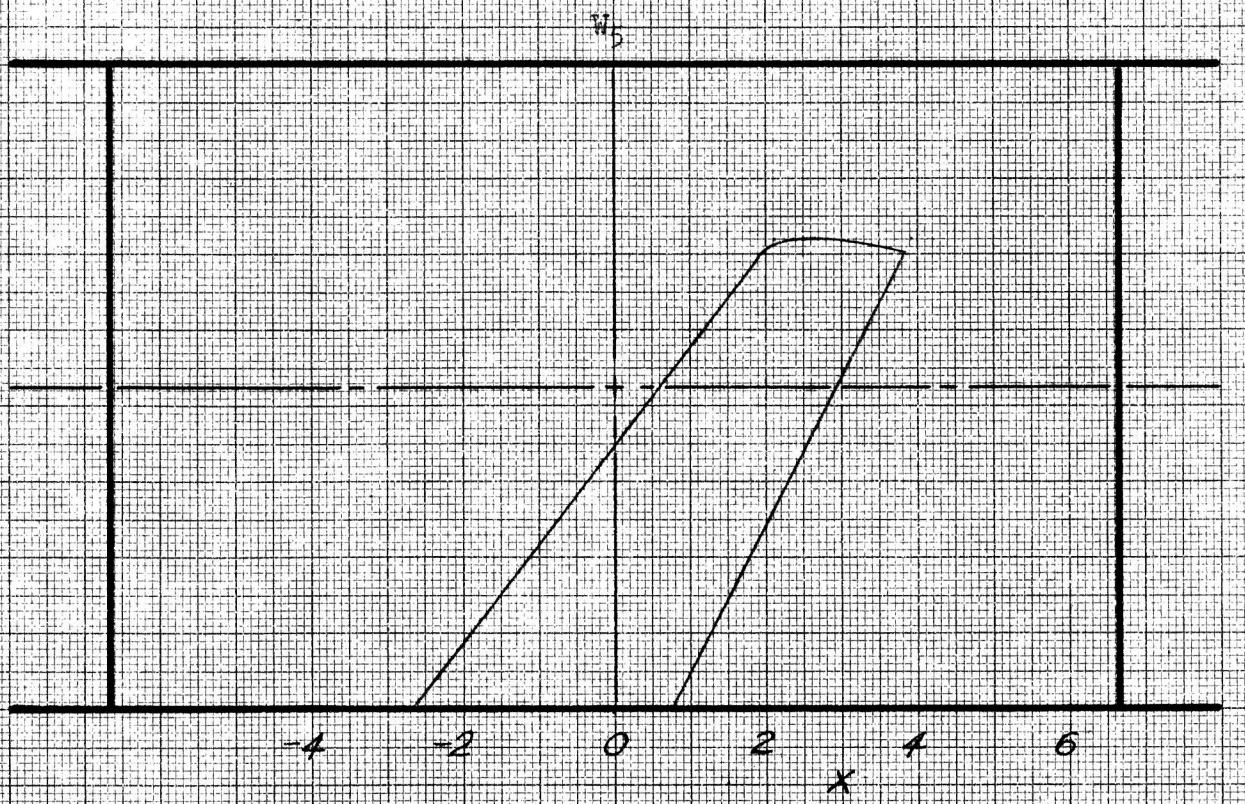

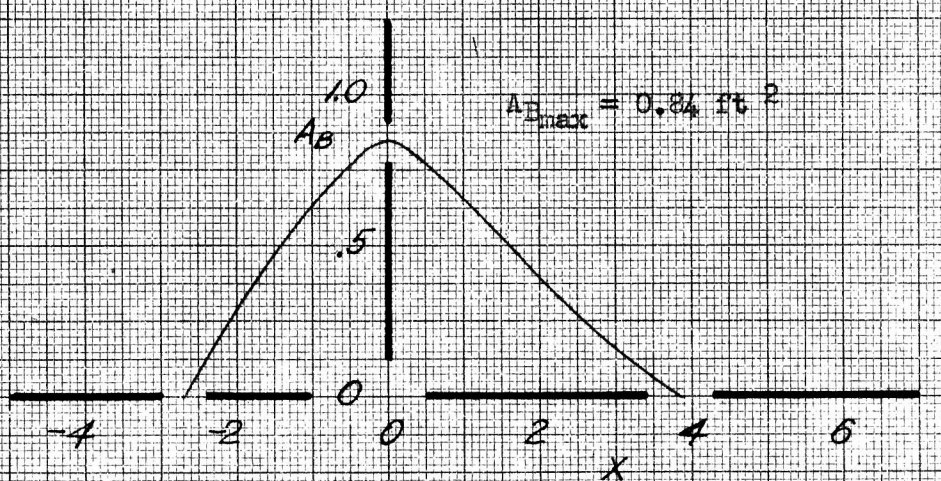

Fig. 7 Sketch of the Model Installation and Plot of the Blocked Area Distribution for W_5

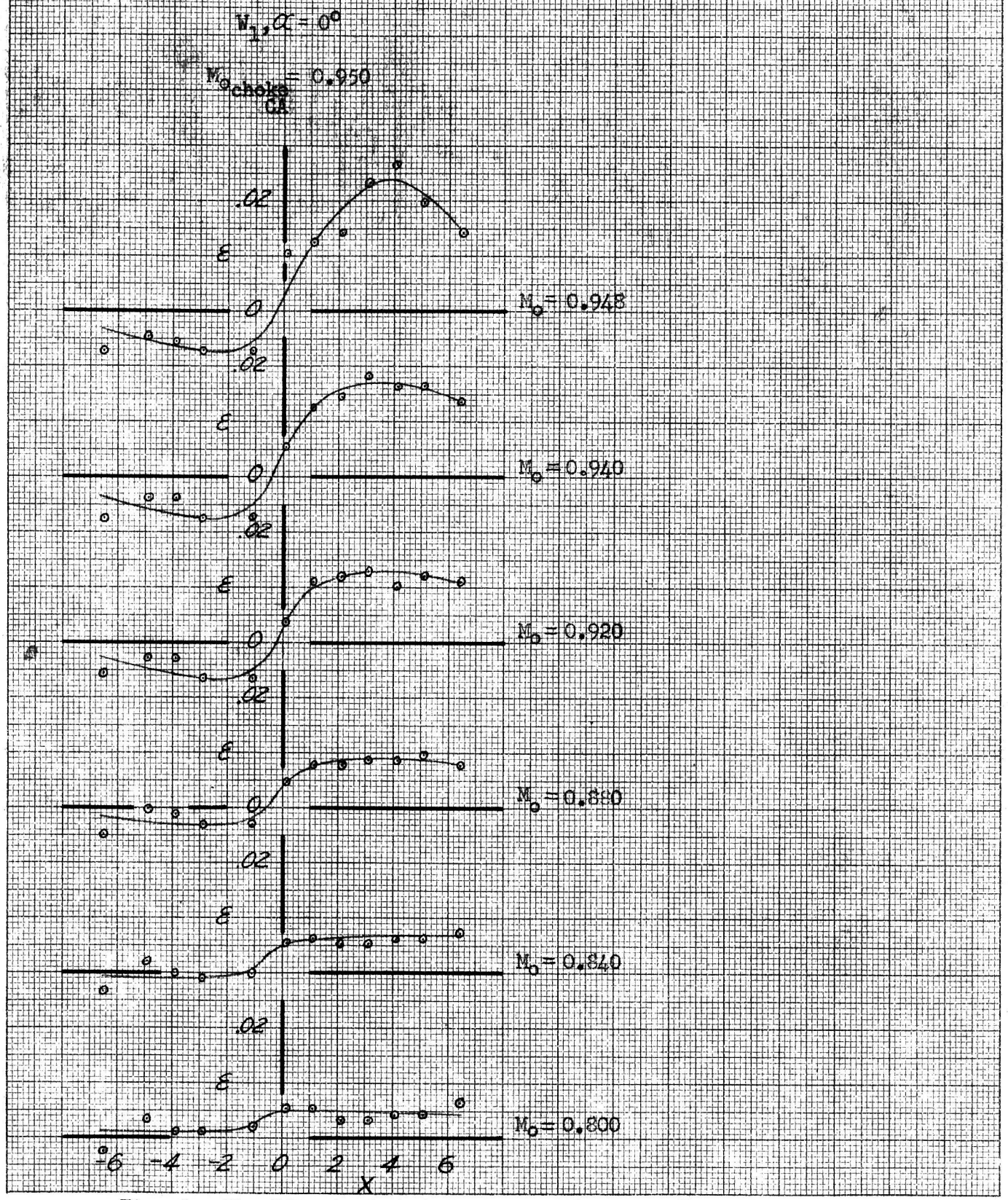

Fig. 8a The Effect of Mach Number on the Axial Variation of Total Blockage at the Wall for W_1 ($\alpha = 0^\circ$), CA

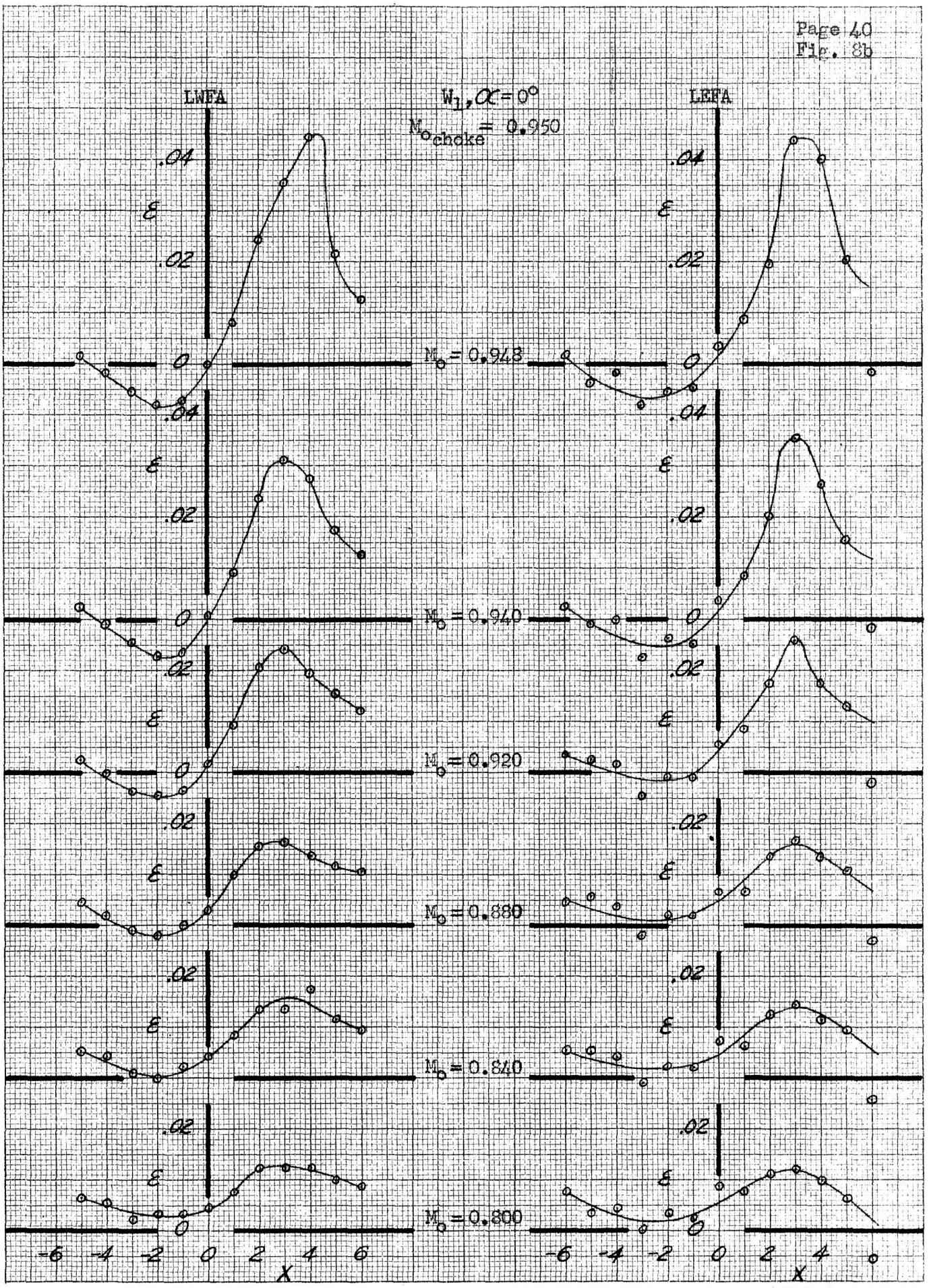

Fig. 8b The Effect of Mach Number on the Axial Variation of Total Blockage at the Wall at Two Positions for W_1 ($\alpha = 0°$), LWFA And LEFA

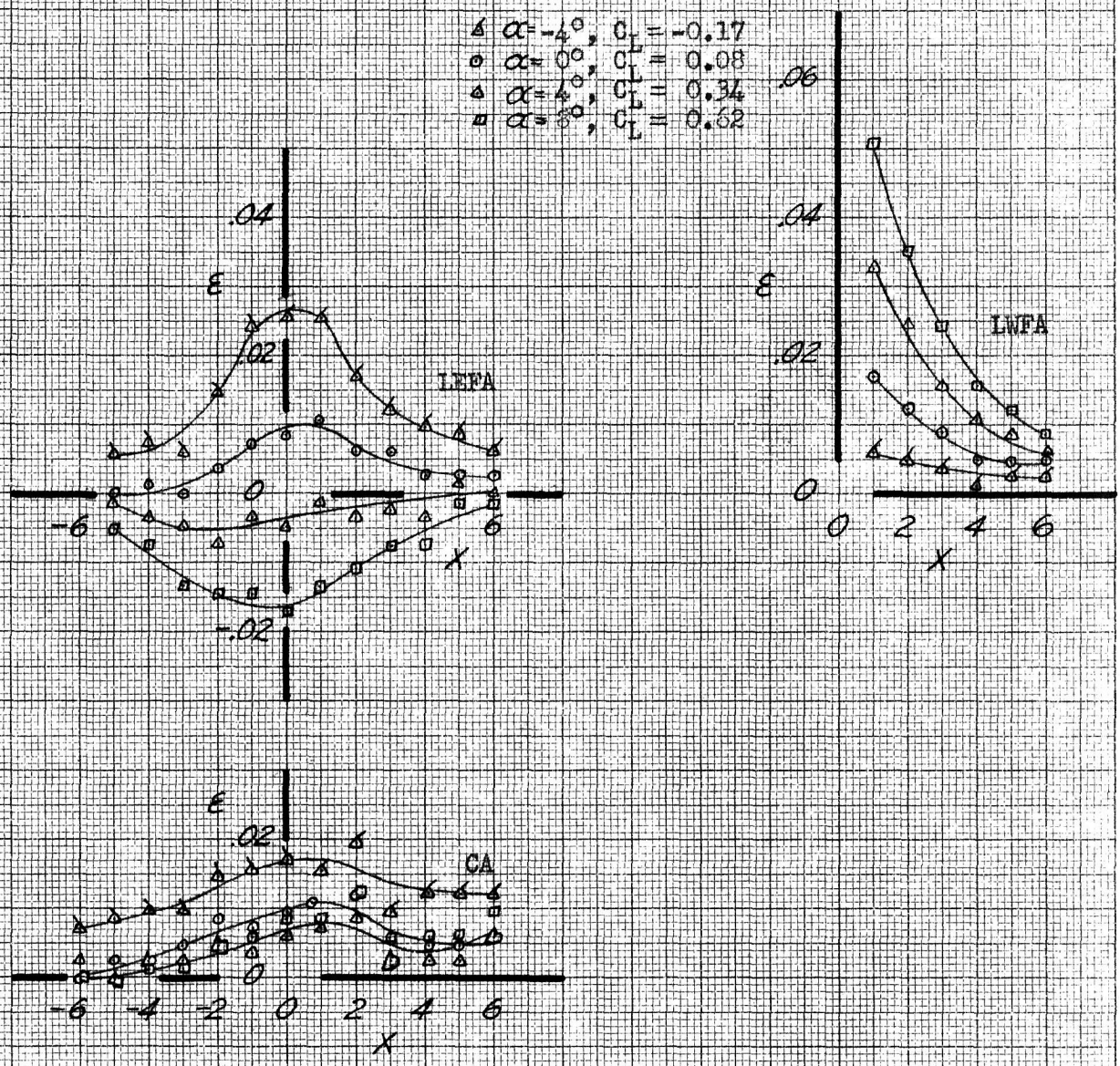

Fig. 9 The Effect of Angle of Attack on the Axial Variation of Total Blockage at the Wall at Several Positions for W_3 ($M_o = 0.740$)

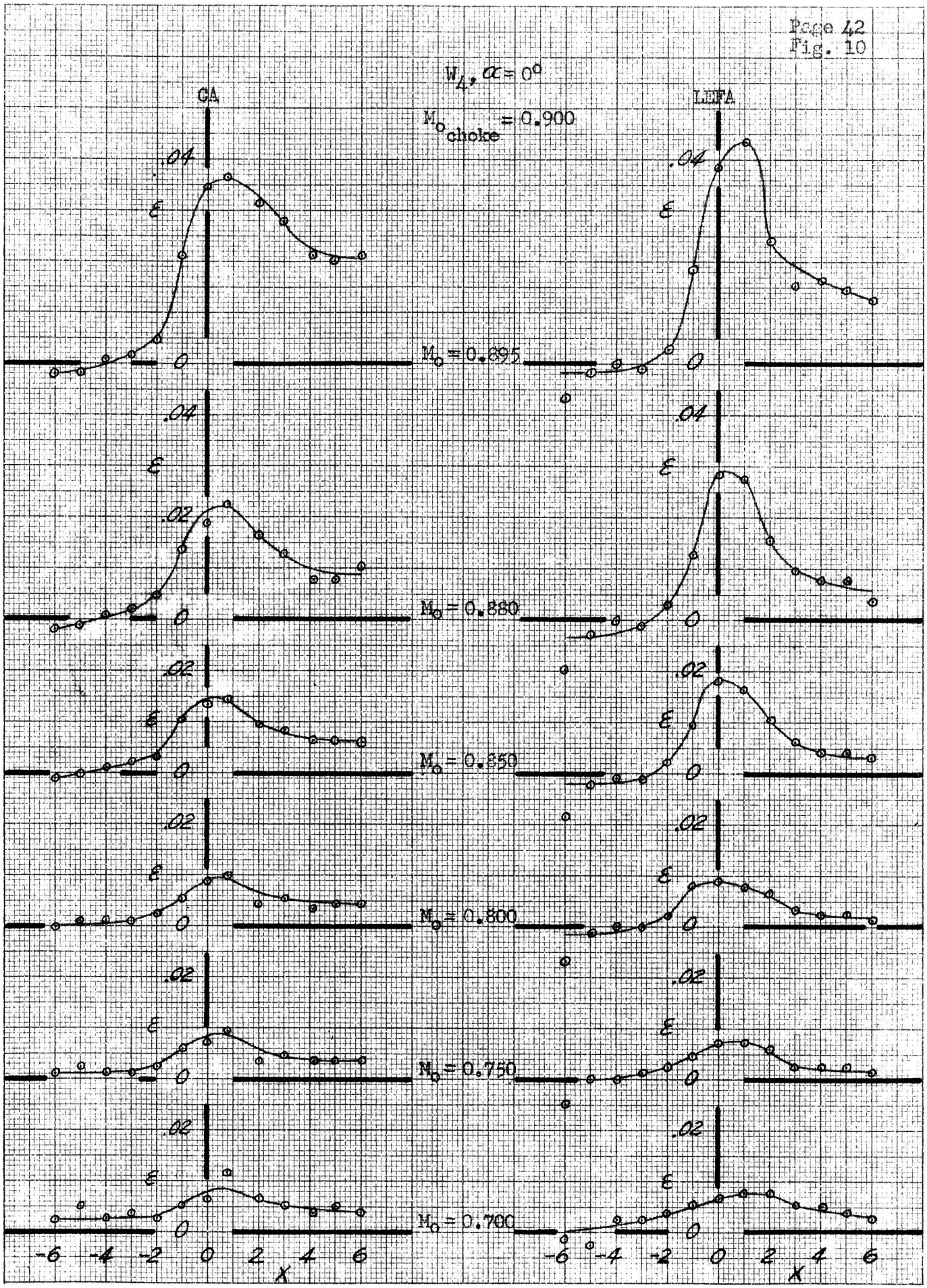

Fig. 10 The Effect of Mach Number on the Axial Variation of the Total Blockage at the Wall at Two Positions for W_4 ($\alpha = 0^\circ$)

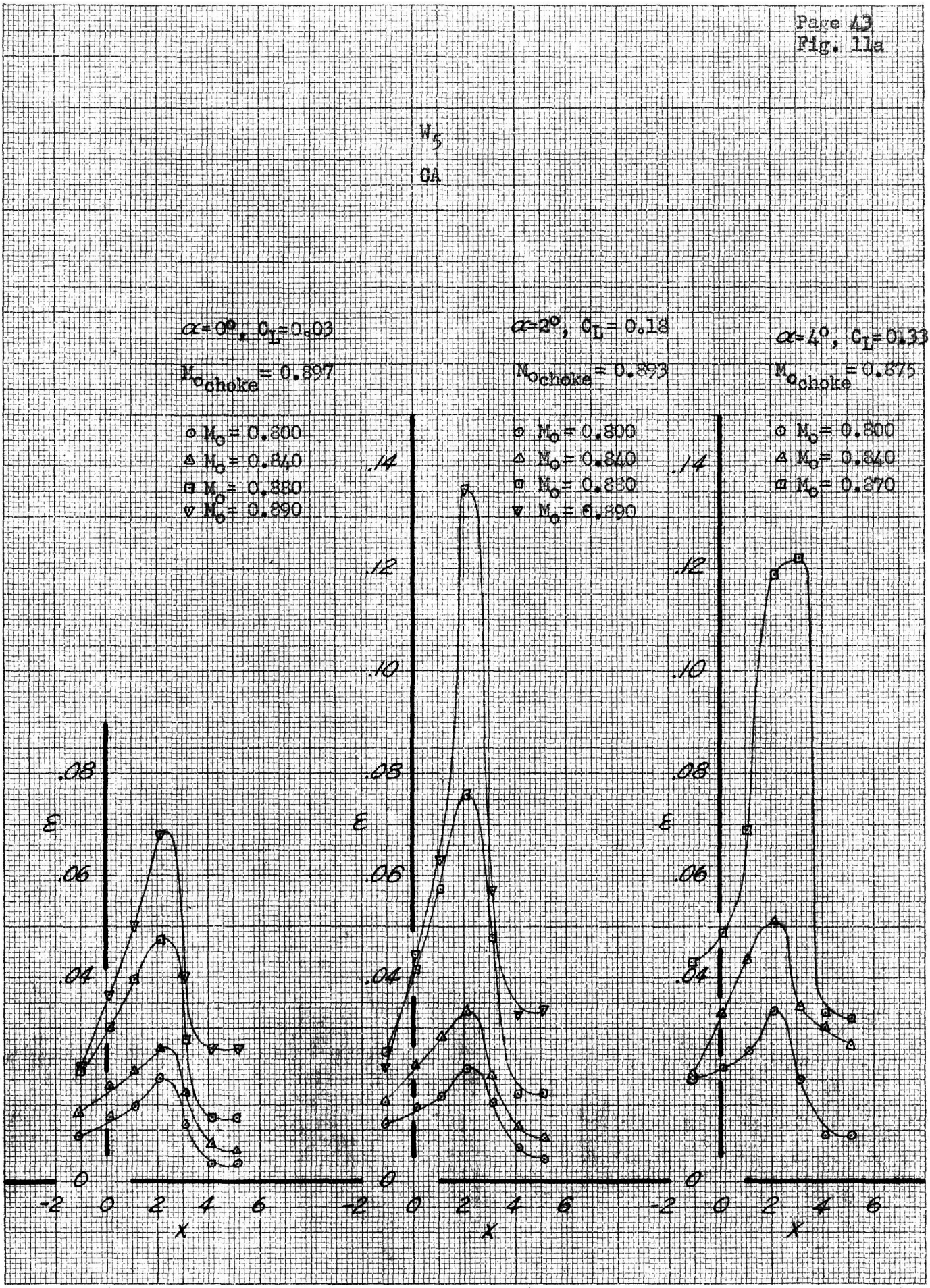

Fig. 11a The Effect of Angle of Attack and Mach Number on the Axial Variation of Total Blockage at the Wall for W_5 (CA)

W_5

LEFA

$\alpha = 0°$, $C_L = 0.03$

$M_{o_{choke}} = 0.897$

- $M_o = 0.800$
- $M_o = 0.840$
- $M_o = 0.880$
- $M_o = 0.890$

$\alpha = 2°$, $C_L = 0.18$

$M_{o_{choke}} = 0.893$

- $M_o = 0.800$
- $M_o = 0.840$
- $M_o = 0.880$
- $M_o = 0.890$

$\alpha = 4°$, $C_L = 0.33$

$M_{o_{choke}} = 0.875$

- $M_o = 0.800$
- $M_o = 0.840$
- $M_o = 0.870$

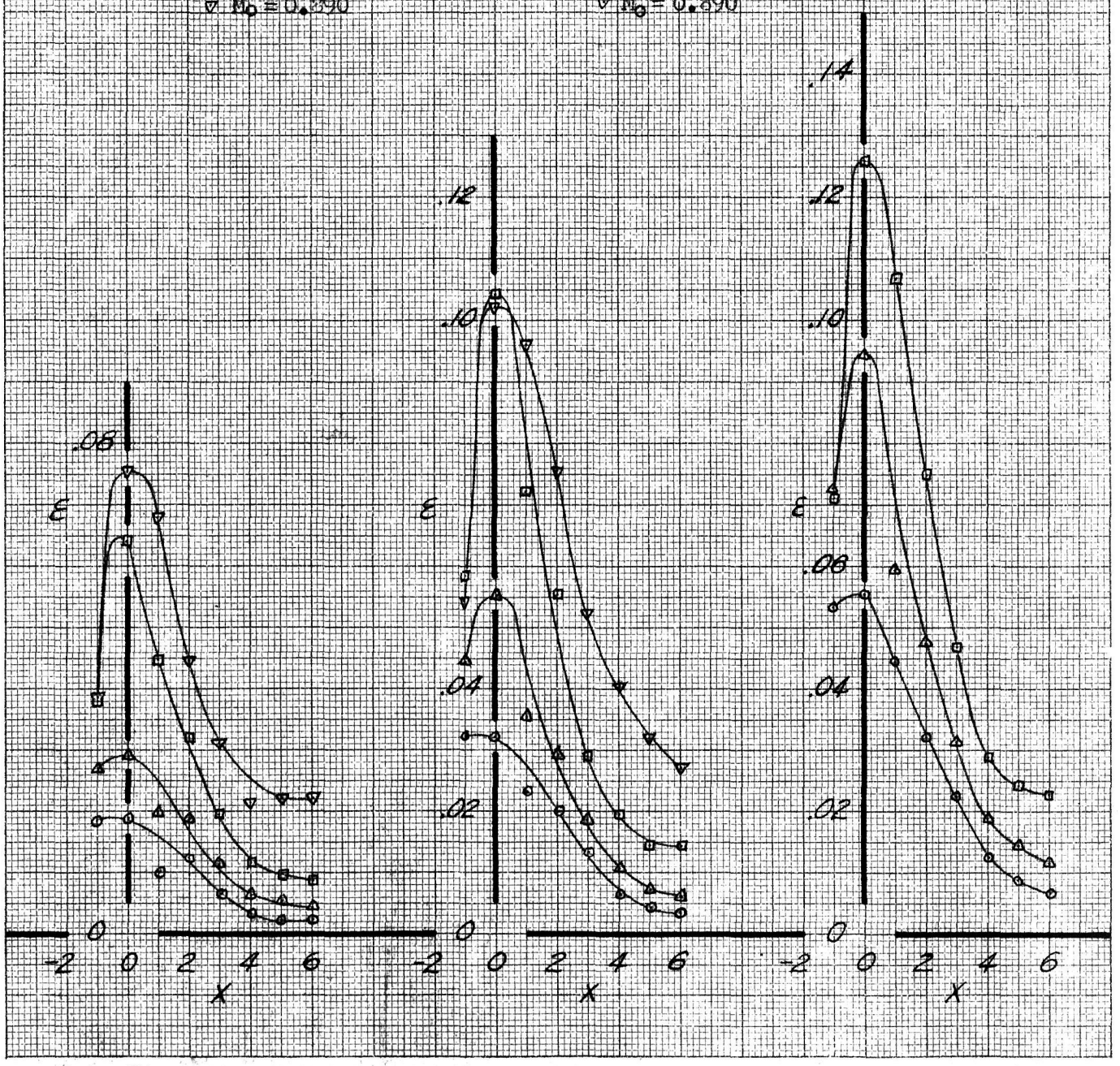

Fig. 11b The Effect of Angle of Attack and Mach Number on the Axial Variation of Total Blockage at the Wall for W_5 (LEFA)

W_5

LWFA

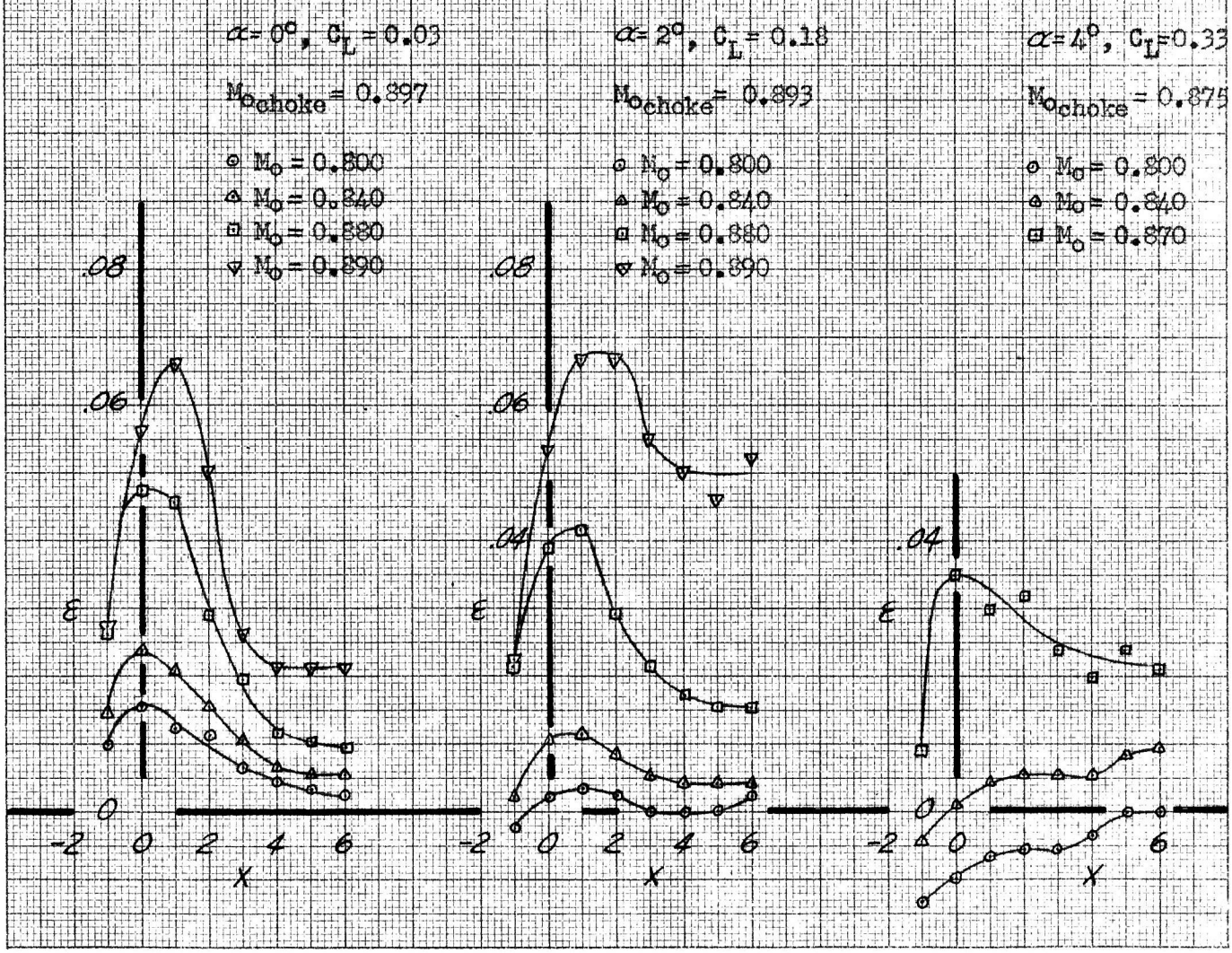

Fig. 11c The Effect of Angle of Attack and Mach Number on the Axial Variation of Total Blockage at the Wall for W_5 (LWFA)

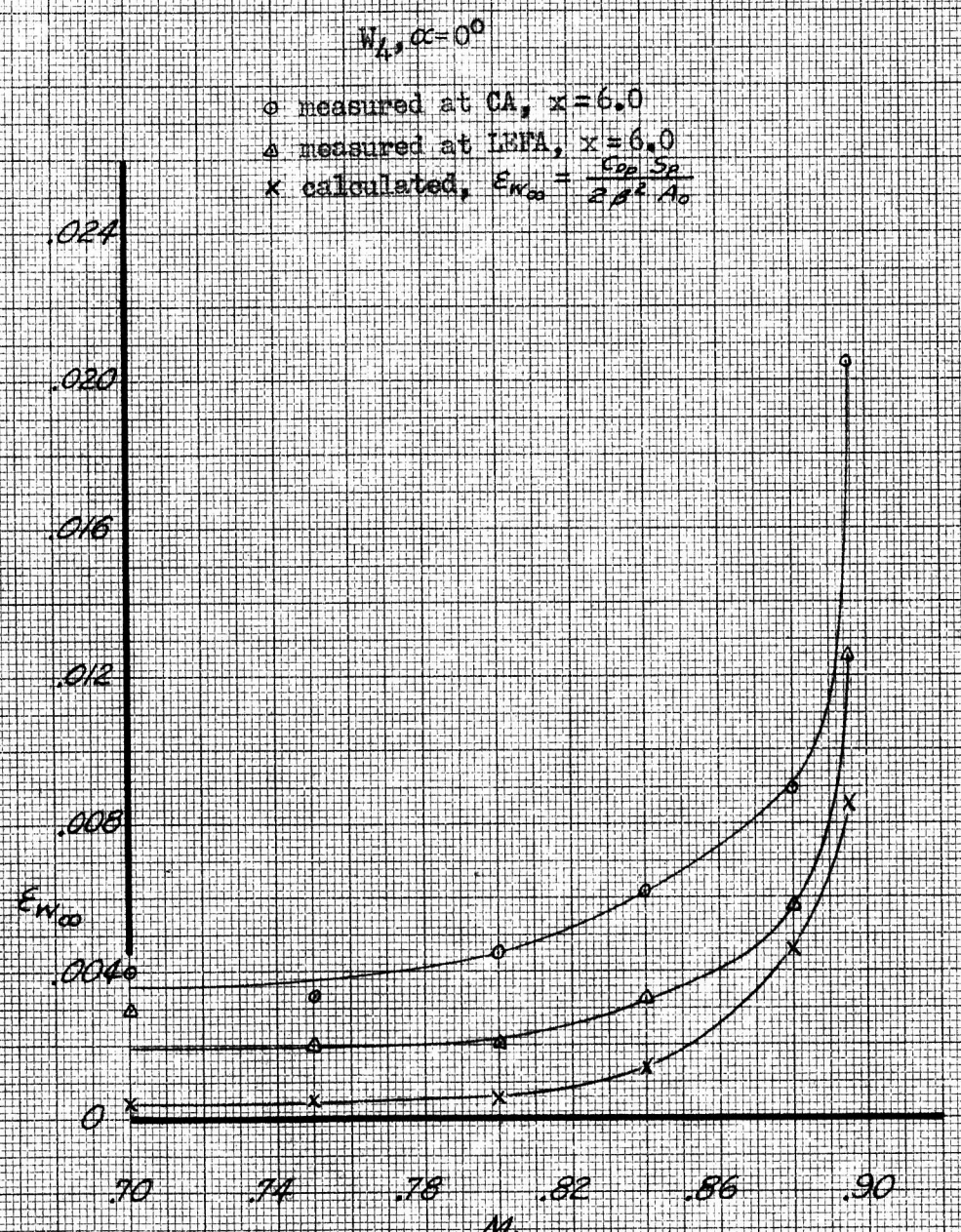

Fig. 12 The Effect of Mach Number on the Comparison of Measured and Calculated Values of Wake Blockage for $W_4, \alpha = 0^\circ$

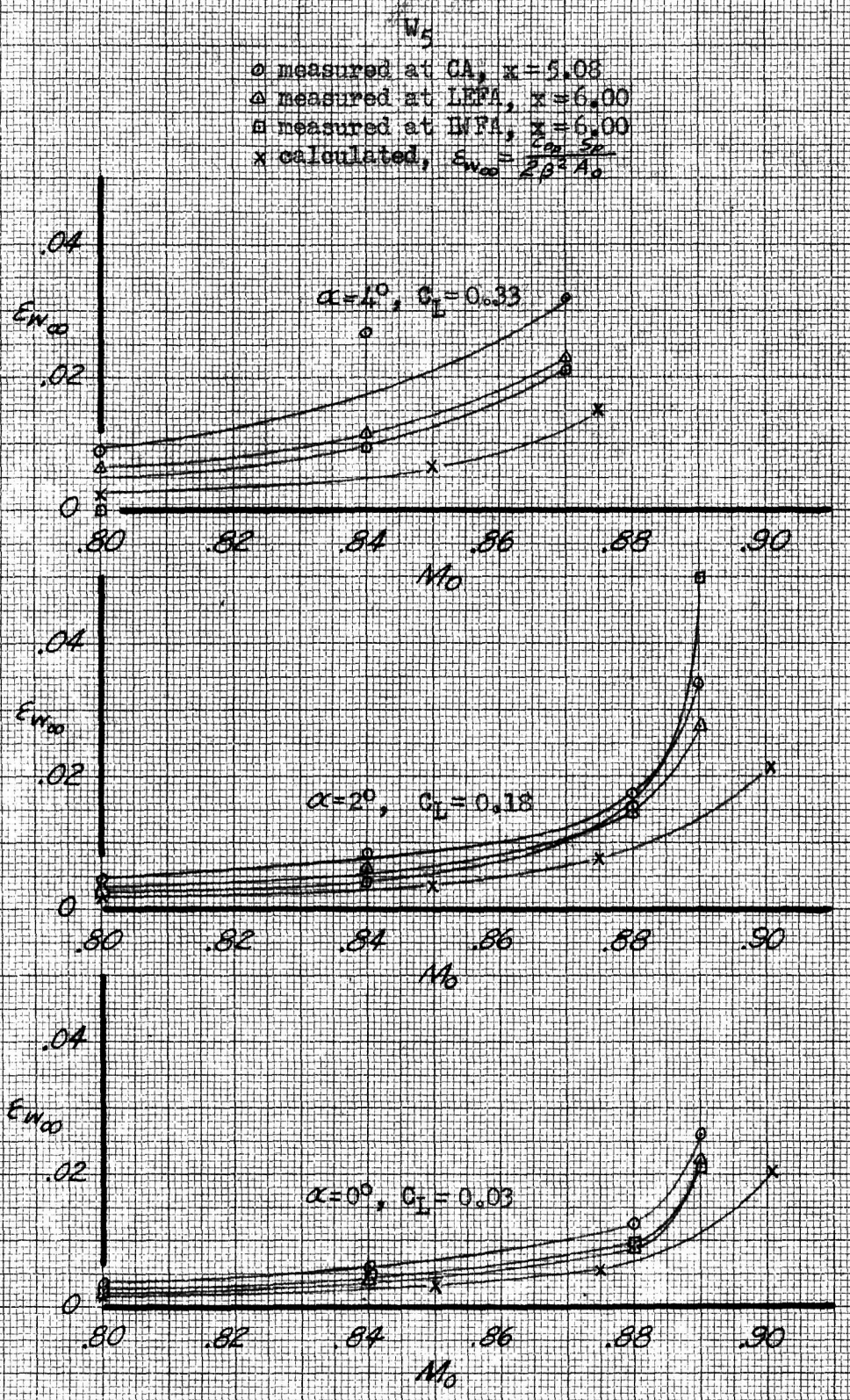

Fig. 13 The Effect of Mach Number on the Comparison of Measured and Calculated Values of Wake Blockage for W_5 at Several Angles of Attack

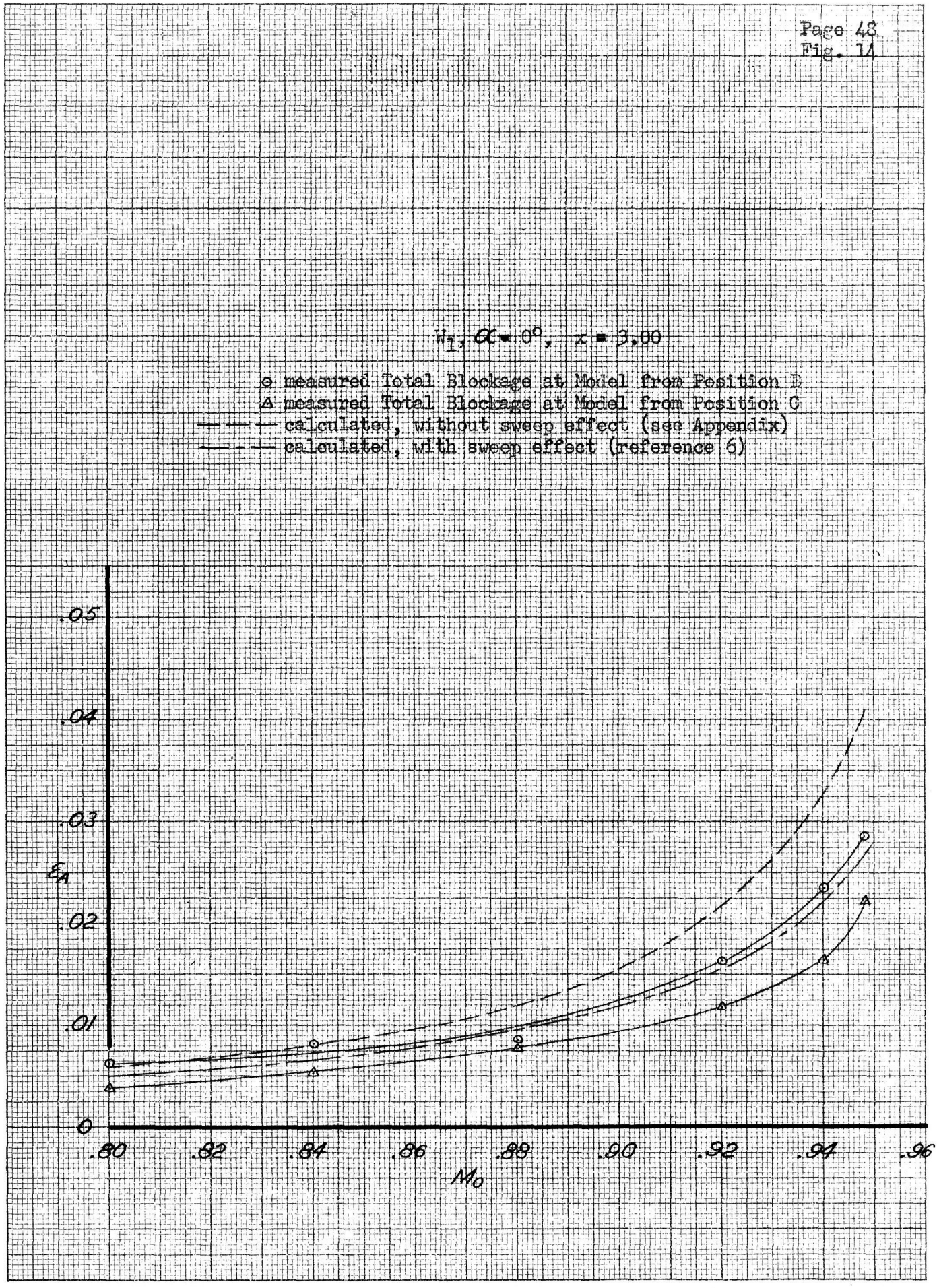

Fig. 14 The Effect of Mach Number on the Comparison of Measured and Calculated Values of Total Blockage at the Model for W_1, $\alpha = 0^\circ$

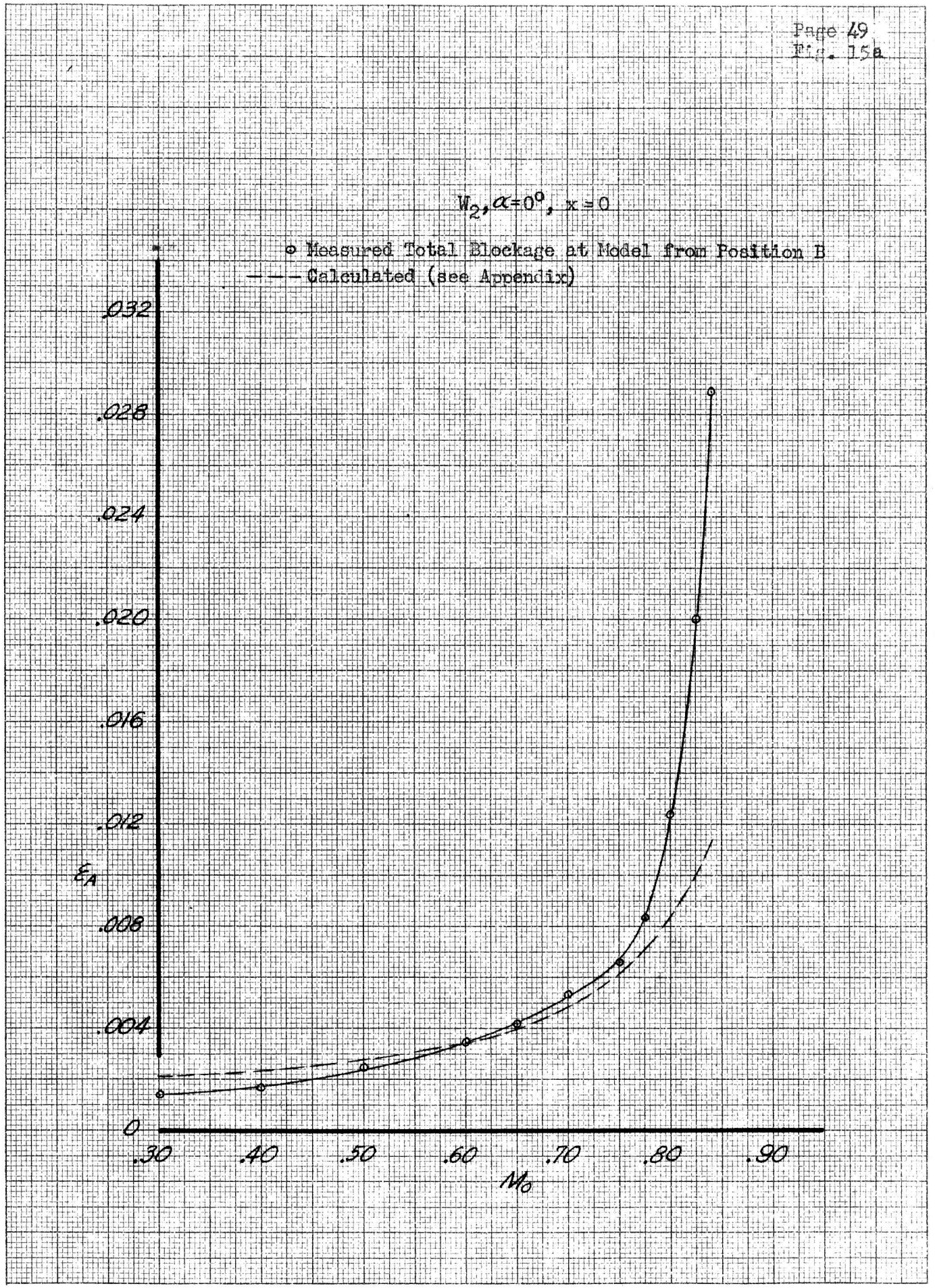

Fig. 15a The Effect of Mach Number on the Comparison of Measured and Calculated Values of Total Blockage at the Model for $W_2, \alpha = 0^\circ$

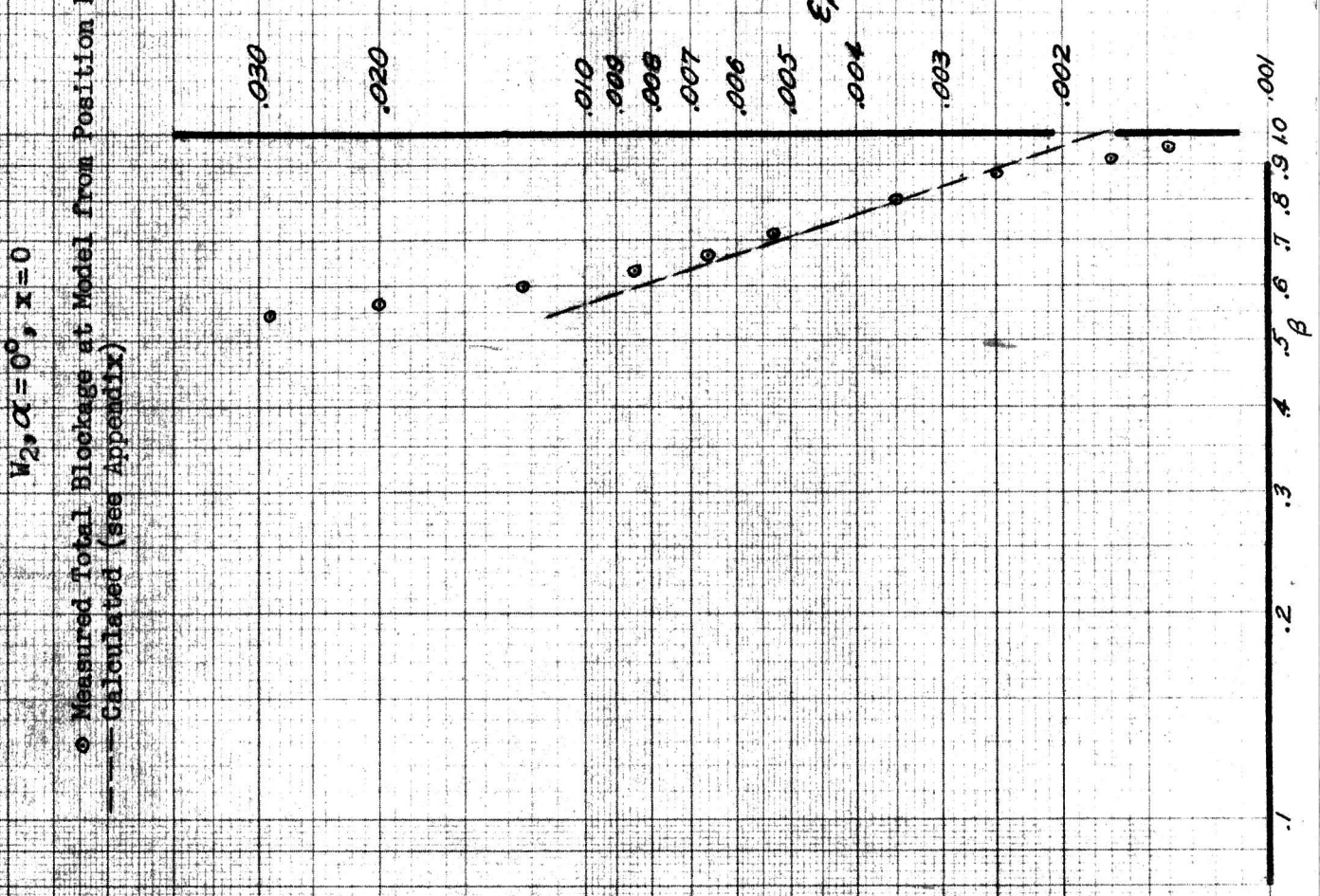

Fig. 15b The Effect of Mach Number on the Comparison of Measured and Calculated Values of Total Blockage at the Model for $W_2, \alpha = 0^\circ$

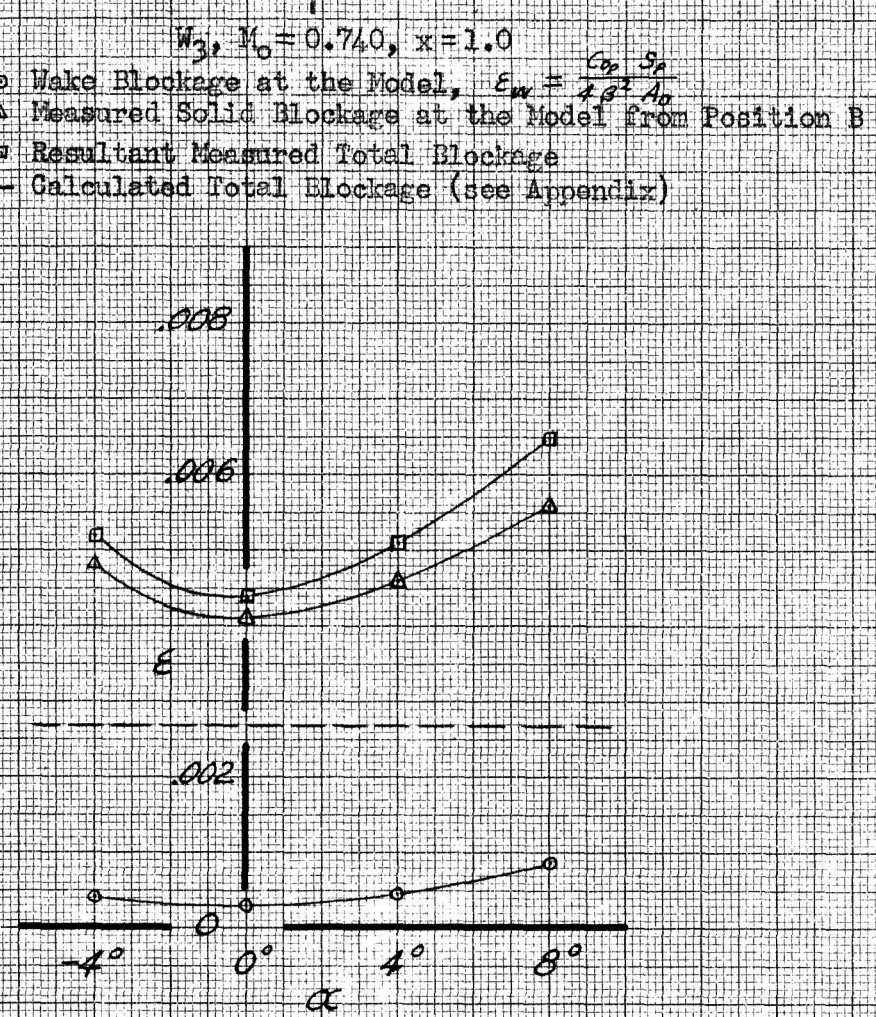

Fig. 16 The Effect of Angle of Attack on the Comparison of Measured and Calculated Values of Total Blockage at the Model for W_3, $M_o = 0.740$

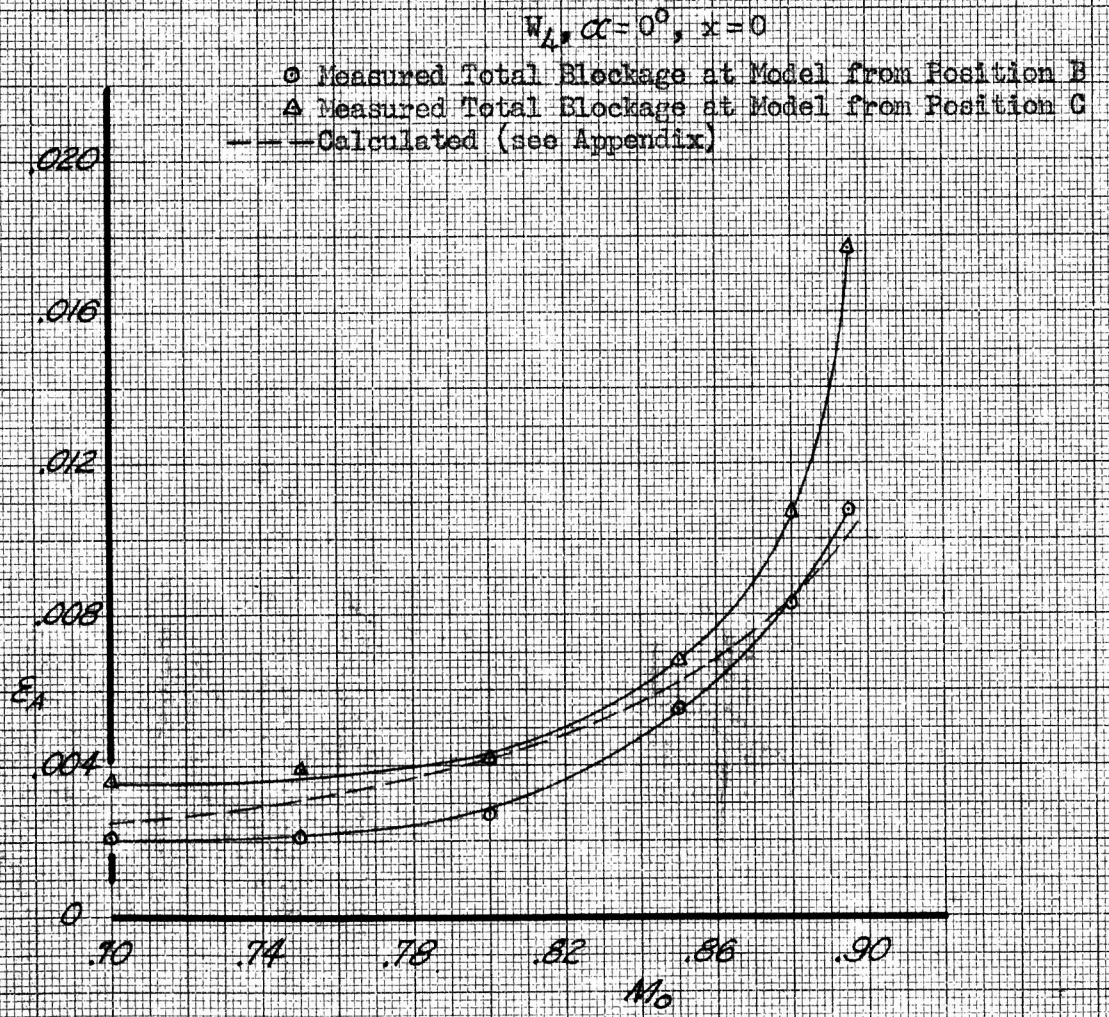

Fig. 17 The Effect of Mach Number on the Comparison of Measured and Calculated Values of Total Blockage at the Model for $W_4, \alpha = 0°$

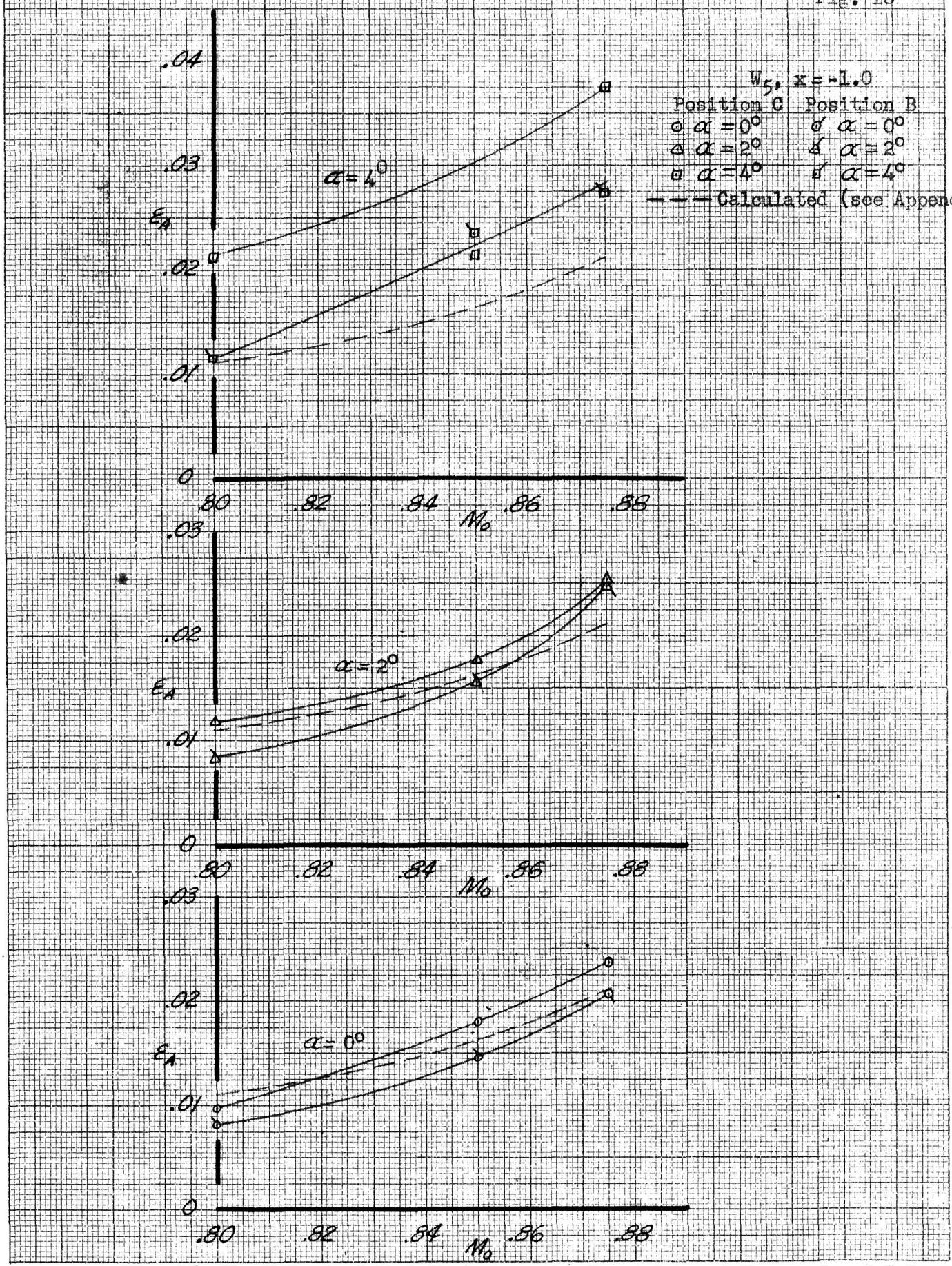

Fig. 18 The Effect of Mach Number on the Comparison of Measured and Calculated Values of Total Blockage at Model for W_5 at Several Angles of Attack

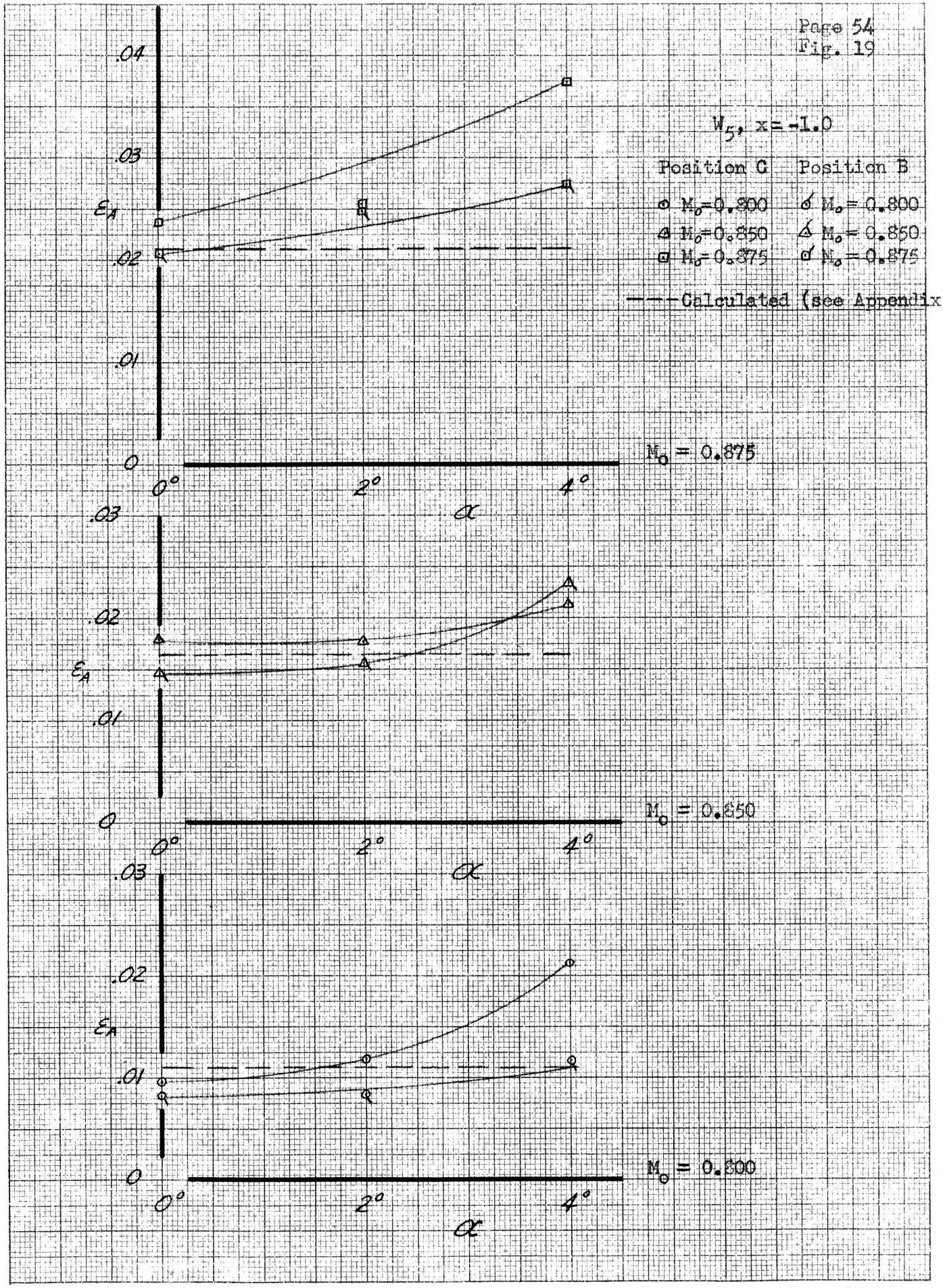

Fig. 19 The Effect of Angle of Attack on the Comparison of Measured and Calculated Values of Total Blockage at the Model for W_5 at Several Mach Numbers

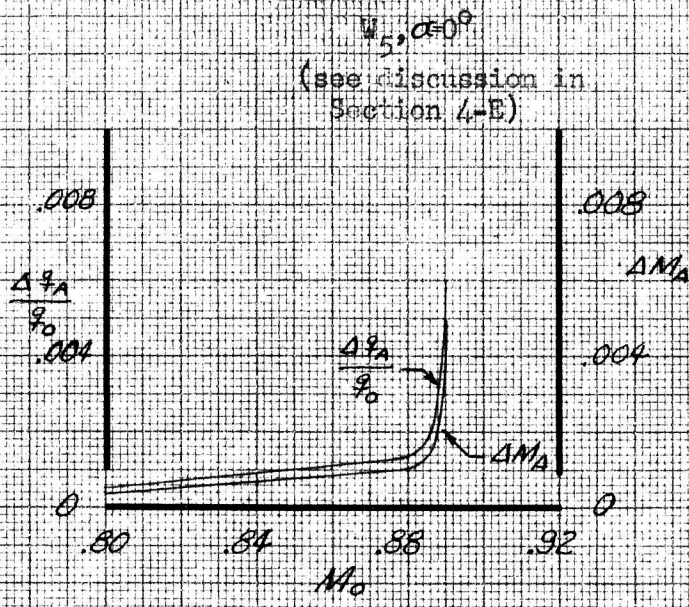

Fig. 20a Increments in Flow Conditions Corresponding to Differences between Measured and Computed Wake Blockage

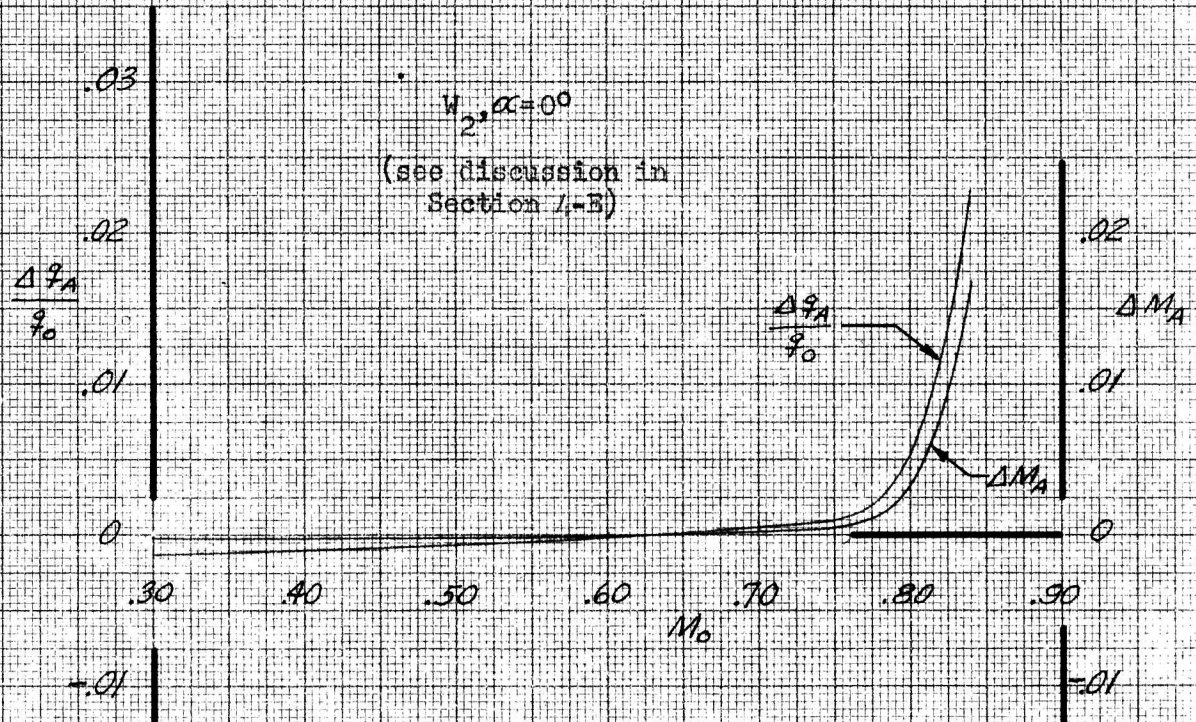

Fig. 20b Increments in Flow Conditions Corresponding to Differences between Measured and Computed Total Blockage

Fig. 20 Increments in Flow Conditions Corresponding to Differences between Measured and Computed Values of Blockage Corrections

APPENDIX

Wake Blockage Equations

The wake blockage at the wing for both two-dimensional and three-dimensional wings may be calculated using the same equation:

$$\varepsilon_{W_A} = \frac{(C_{D_p})(S_p)}{4 A_o} = \frac{1}{4 A_o} \frac{\text{Drag}}{q} = .0026\, C_{D_p} S_p \quad \text{(for CWT)}$$

The wake blockage far downstream from the wing is given by the equation:

$$\varepsilon_{W_\infty} = \frac{(C_{D_p})(S_p)}{2 A_o} \quad \text{or} \quad \varepsilon_{W_\infty} = 2\varepsilon_{W_A}$$

This is a direct consequence of the uniform flow from infinity plus the image and primary sources in the plane of the model.

The wake blockage for compressible flow is $\frac{1}{\beta^2}$ times the values given above.

Solid Blockage Equations

1. Two-dimensional Wings

The solid blockage at the model is given by the following equation:

$$\varepsilon_{s_A} = \frac{0.77\, \pi\, ct}{6 H^2} \quad \text{(wing spanning tunnel horizontally)}$$

$$\varepsilon_{s_A} = \frac{0.77\, \pi\, ct}{6 B^2} \quad \text{(wing spanning tunnel vertically)}$$

The solid blockage for compressible flow is $\frac{1}{\beta^3}$ times the values given above.

2. Three-dimensional Wings

The solid blockage at the wing mounted centrally in the tunnel is:

$$\varepsilon_{s_A} = \frac{0.775\ (\text{model volume, ft}^3)}{H^2 B} = .0010\ (\text{volume, ft}^3) \quad \text{(for CWT)}$$

This equation includes a correction for the fillets in the CWT working section.

The solid blockage at a reflection plane wing is:

$$\varepsilon_{s_A} = \frac{0.775 \text{ (model volume, ft}^3\text{)}}{\sqrt{2}\, H^2\, B} = .0007 \text{ (volume, ft}^3\text{)} \quad \text{(for CWT)}$$

The solid blockage for compressible flow is $\frac{1}{\beta^3}$ times the values given above.

Total Blockage Equations

The total blockage is the sum of wake blockage and solid blockage:

$$\varepsilon = \varepsilon_s + \varepsilon_w$$

The total blockage for compressible flow is then:

$$\varepsilon = \frac{(\varepsilon_s)_{M_o=0}}{\beta^3} + \frac{(\varepsilon_w)_{M_o=0}}{\beta^2}$$

The equations used to calculate all of the "computed" blockage values is an approximation to the above relation, namely,

$$\varepsilon_A = \frac{1}{\beta^3} (\varepsilon_A)_{M_o=0} \qquad \text{where} \qquad (\varepsilon_A)_{M_o=0} = \left(\varepsilon_{s_A} + \varepsilon_{w_A}\right)_{M_o=0}$$

The approximation is that $C_{D_p} = \frac{\left(C_{D_p}\right)_{M_o = 0}}{\beta}$

Mach Number and Dynamic Pressure Corrected for Blocking

The increment in Mach number due to blocking is given by the equation:

$$\Delta M_A = M_o \varepsilon_A (1+0.2\, M_o^2)$$

The ratio of the increment in dynamic pressure to the dynamic pressure of the undisturbed airstream is given by the equation:

$$\frac{\Delta q_A}{q_o} = \varepsilon_A (2 - M_o^2)$$